IEEE Access
Multidisciplinary ⋮ Rapid Review ⋮ Open Access Journal

Received 26 October 2023, accepted 14 November 2023, date of publication 20 November 2023,
date of current version 27 November 2023.

Digital Object Identifier 10.1109/ACCESS.2023.3334685

RESEARCH ARTICLE

Graphene-Based Surface Plasmon Resonance Sensor for Water Salinity Concentration Detection Using Multiple Light Source Techniques

KHANDAKAR MOHAMMAD ISHTIAK, SAFAYAT-AL IMAM, (Member, IEEE), AND QUAZI D. M. KHOSRU

Department of Electrical and Electronic Engineering, Bangladesh University of Engineering and Technology, Dhaka 1205, Bangladesh

Corresponding author: Quazi D. M. Khosru (qdmkhosru@eee.buet.ac.bd)

This work was supported by the Department of Electrical and Electronic Engineering, Bangladesh University of Engineering Technology (BUET).

ABSTRACT A Graphene-based surface plasmon resonance sensor is proposed for rapid water salinity concentration detection and operates with a new multiple light source technique. The proposed sensor consists of a CaF_2 prism coupled with incident light of five different wavelengths. This multiple-source technique significantly increases the sensor detection accuracy and overall performance for the 1% to 30% water salinity concentration detection. The proposed sensor achieved a noticeably higher value sensitivity of 397.71 (deg./RIU), a Quality Factor of 99.50 (1/RIU), and a Figure of Merit of 94.82. The sensor also obtains a wide range of detection accuracy of 0.199 to 0.498 (1/deg.) while maintaining a considerably low minimum reflectance of 0.05 (normalized) for the whole salinity detection range. In addition, all of those performance parameters and results are compared to the most recent relevant works. The proposed salinity sensor obtained a significantly high sensitivity, a wide range of detection accuracy with higher efficiency, and overall improved performance. This impressive performances of the proposed Graphene-based SPR sensor for measuring water salinity level exhibited the highest sensitivity, wide range, high accuracy, efficiency, and reliability to detect water salinity concentration.

INDEX TERMS Graphene, sensor, surface plasmon resonance, salinity concentration, sensitivity, quality factor, figure of merit, detection accuracy.

I. INTRODUCTION

Water is the most crucial substance for human survival. Human cells contain about 70% water, making up the majority of the human body. Pure drinking water is the foundation from which all bodily fluids are derived, including blood, lymph, saliva, digestive enzymes, urine, etc. [1].

Water's potential utility extends to all forms of life, including providing humans with a safe and reliable drinking water supply and helping farmers with their agricultural irrigation needs. Almost 97% water on Earth is salt water, only 3% is fresh water is drinkable [2], [3]. More over two-thirds of the fresh water on Earth is locked up in glaciers and polar ice caps. The majority of the remaining unfrozen freshwater is contained in underground aquifers, with only a trace amount found in the atmosphere or on the surface.

Water is getting increasingly scarce and polluted on Earth. Population expansion, industrialization, and climate change are all contributing to a global water crisis. As a result of global warming, the weather has changed and the sea level is rising at an alarming rate. The current rate of increase is 4.62 mm per year (or 0. 0.182 inches), which is expected to continue increasing in the future [4]. As one moves closer to the seaside, the water supply changes, becoming saltier. It has serious consequences for food production and drinking water.

Salinity in water is detrimental to the health of all kinds of life. Water's salinity must be lowered before it can be utilized for human consumption, agricultural

The associate editor coordinating the review of this manuscript and approving it for publication was Mauro Fadda.

irrigation, or manufacturing. The mass ratio of the dissolved components in a particular volume of saltwater is known as its absolute salinity and is expressed in milligrams per kilogram or parts per thousand. In general, saltwater with a salinity of 35% at 0° is considered to be neutral [5]. The amount of oxygen that can be found in water depends on its salinity. As salt content rises, less oxygen can be dissolved in the liquid medium. In comparison at the same temperature, the oxygen solubility in seawater is approximately 20% lower than in fresh water. Consuming salt water has been linked to number of medical issues, including high blood pressure, diarrhea, cholera, skin infections, slow new-born growth, and even death. So, it is crucial to determine the salinity level before consuming, farming with, or otherwise utilizing the water for health-related purposes.

Water salinity is traditionally measured using the electrical conductivity of chloride ions since conductivity is proportional to ion concentration. However, this method of measurement is compromised by interference from other contaminating ions [6], [7]. This technique is vulnerable to corrosion and current instability as a result of electrolysis. Recently, ultrasonography and chemical reactions have been established as innovative approaches to characterizing salinity. There are several other techniques that can be used, such as gravimetric analysis and chlorinity titration. Gravimetric determination involves evaporating a sample of water and then weighing the dry residue to determine its salinity. All of these methods of measurement are used to determine saline levels with great precision, however they all necessitate the use of an expert's hand and are not portable.

Optical methods are one of the most promising strategies that traction the scientists and researchers for use in a variety of sensors and biosensor devices. Surface plasmon resonance (SPR) technique is one of the optical methods which gained the attention of scientists for water salinity detection due to its many advantages over other methods, such as its high sensitivity, very high detection accuracy and fast response to minute changes in the refractive index of the sensing layer analyte, its need for only a small amount of sample, its repeatability, its absence of labels, and its real-time detection capabilities [8], [9], [10], [11], [12], [13], [14], [15]. The SPR techniques rely on the correlation between the refractive index and salt concentration in saltwater [16].

There are various type of surface plasmon resonance based optical sensors depending on the structure pattern and applied-light coupling techniques. Diffraction-coupled, waveguide-combined, prism-paired and fiber-optic SPR sensors are only few of the many types of SPR sensors available [17], [18], [19], [20]. The prism-coupled SPR sensors are simple to manufacture, they are recommended over fibre optic SPR sensors. There are two types of configurations are used in SPR technique, Kretschmann configuration and Otto configuration [21], [22]. The Kretschmann apparatus uses a metal coating on a prism's surface to simulate directed or dripping waves, whereas in the Otto setup, air is employed to mimic errant or faulty waves. When an electromagnetic (EM) wave penetrates a material at an angle larger than its critical angle, it excites surface plasmon polaritons, which in turn form surface plasmon waves (SPWs) at the prism-metal (P-M) interface (SPPs). When the wave vector of the evanescent wave (EW) and the SPW at the metal-dielectric (M-D) contact are the identical, the SPWs will excite the EW. The EW intensity rapidly decreases in directions perpendicular to the P-M contact [23]. As a result, the SPWs then oppose the plasmon and converting its light energy into reflected light. Resonant oscillations of SPW are influenced by the surface refractive index (RI), leading to poor reflectivity [24]. This means that the SPR sensor may pick up extremely subtle shifts in the amount of reflected light. The sensitivity (S) and figure of merit (FOM) analyses as well as the Attenuated total reflection (ATR) method were employed to evaluate the RI shifts [24]. Using SPWs-oriented SPR, scientists have shown that the angular interrogation method reliably yields precise sensitivity ratings for any detection method [25], [26], [27], [28].

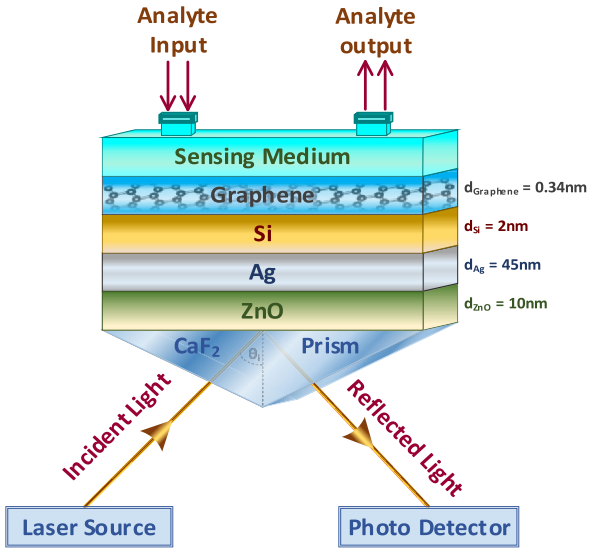

FIGURE 1. The proposed SPR biosensor for salinity concentration n detection.

According to the literature review, the surface plasmon resonance-based sensor can designed to detect particular targeted objects like – different cancer cells, different types of bacteria and virus, different types of gas or chemical, etc., where an analyte is used as a layer to trap or bond the targeted sample to detect [11], [27], [28], [29], [30], [31], [32], [33]. The analyte layer is a material that has optical properties, which means refractive index. When a targeted sample is attached or creates a bond with the analyte, the refractive index of the analyte changes. This variation is not directly measurable. Then, the sensitivity is measured or detection is done by measuring the relativity response curve for changing the background media's refractive index [27], [28], [29], [30], [31], [32], [33]. There is another type of surface plasmon resonance-based sensor which is used to

detect and measure the sample values such as - hemoglobin level in the blood, glucose level in blood, glucose level in urine and chemical concentration levels, etc., where need to measure different concentration level based on the applied sample to the sensing medium [10], [12], [34], [35], [36], [37], [38]. The concentration level of the sample is directly related to the refractive index of the sample. The sensor needs to be calibrated with sample data sets to measure the concentration level accurately. Due to this reason, the sensor design needs to be analyzed and optimized with predefined or known data sets. Due to this reason, the sensor design needs to be analyzed and optimized with predefined or known data sets. The target of the proposed design is to achieve the highest possible detection accuracy and overall performance. Therefore, the proposed structure is analyzed and calibrated with a known data set for accurate detection and precision measurement of the applied sample.

This paper presents a new surface plasmon resonance biosensor based on thin graphene layer for rapid detection of water salinity level with very high sensitivity and accuracy. The proposed sensor is consisting of five different layers as order of prism, ZnO, Ag, Si and Graphene. A CaF_2 prism is connected to the biosensor as a substrate, which couples incident light of five different wavelengths - 633nm, 643.8nm, 690nm, 700nm, and 720nm. This new multiple source technique significantly enchanted the sensor performance to detect the water salinity with very high detection accuracy. This sensor is capable of measuring 1% to 30% water salinity concentration at a constant pressure of 0 kg/cm^2 and a temperature of 20°C for all five different wavelengths of incident light sources, which greatly increases the accuracy of the salinity detection. In a sensing medium, the surface refractive index will shift due to the presence of salt water. To detect the presence of salt water, the salinity concentration is determined by measuring this change in the sensing medium and comparing it to other performance metrics. The proposed new SPR salinity sensor demonstrated the maximum sensitivity, quality factor, full width at half maximum, figure of merit, and detection accuracy for water salinity concentration level detection.

II. DESIGN MODEL AND METHODOLOGY

In this section, we describe the design considerations and methodology for the proposed water salinity concentration sensor.

A. DESIGN CONSIDERATION OF SPR SALINITY SENSOR

Fig. 1 present a Graphene-based SPR water salinity sensor structure. The proposed SPR sensor has five layers, the first layer of which is a CaF_2 prism. As a substrate, a CaF_2 prism couples incident light with five distinct wavelengths (λ) of 633nm, 643.8nm, 690nm, 700nm, and 720nm. In the realm of optical sensors, the refractivity of the prism has a direct effect on the sensor's sensitivity. With a minor change in the sensing medium, a prism with a low RI can attain a larger change in angle of reflection [29], [39]. Using a prism with a lower RI will allow for greater sensitivity. Prisms of the BK7, FK51a, SF10, and SF11 types are the most popular and commonly used. In comparison to other prism materials, CaF_2 prisms have a relatively low RI [30].

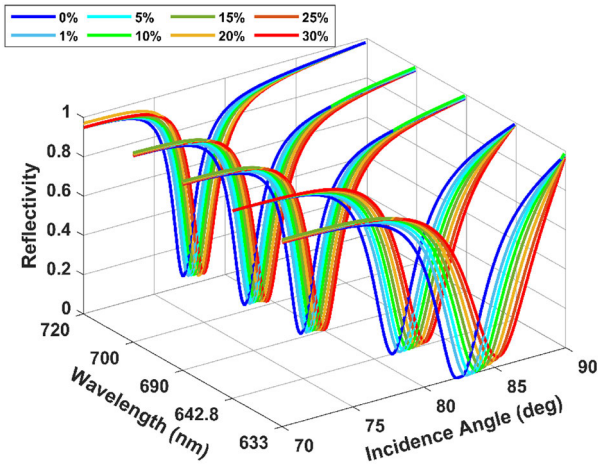

FIGURE 2. 3D representation of the relation between reflectivity, incident angle and incident light wavelengths with 0% to 30% water salinity variation.

The second layer consists of a $d_{ZnO} = 10$ nm thin ZnO layer as deposited on the CaF_2 prism's surface. The ZnO-based sensor demonstrates substantially higher performance parameters than conventional sensors [31]. Due to poor adhesion between the metal layer and the prism, SPR biosensor sensitivity is reduced [40]. Compared to other adhesion materials like Cr, Cu, etc. [41], several studies have shown that ZnO, which functions as an active adhesive layer between the prism and the metal layer, significantly boosts the sensor's performance when it comes to SPR measurements [42]. In order to counteract this loss of sensitivity, a layer of ZnO was placed on top of the CaF_2 prism. Large changes in resonance angle are caused by the ZnO layer's increased plasmonic impact through effective light trapping and augmentation of light trapping capabilities [43]. Additionally, the ZnO layer also protects the silver layer from oxidation [44].

Traditional SPR biosensor architecture frequently uses a thin surface of plasmonic materials for the SPR sensor. Plasmonic materials, such as gold (Au) and silver (Ag), etc., are deposited on top of the prism or separated from it by a thin oxide layer to facilitate the propagation of SPs [45], [46]. These materials have a sharply-sharpened reflectance curve that is narrow in the near-infrared and infrared range (IR), making them particularly sensitive [47]. Because it exhibits a stronger resonance angle change in response to the RI variance of the sensing medium and offers a higher sensitivity, gold is preferred as a metal layer for SPR sensors. In various conditions, gold is more resistant to oxidation and corrosion, which suggests inertness and chemical stability [48], [49]. The disadvantage, however, is that biomolecules do not adhere well to gold, which reduces the sensitivity of

TABLE 1. Refractive index and corresponding water salinity concentration for proposed SPR sensor.

Water salinity concentration (%)	0%	1%	5%	10%	15%	20%	25%	30%
Refractive Index	1.33	1.33175	1.33266	1.33357	1.33447	1.33538	1.33629	1.33699

the traditional SPR biosensor. Alternatively, silver (Ag) thin film employed in SPR sensor as a sensing substrate yields superior accuracy than gold because silver produces sharpest SPR peak with stronger contrast, i.e. the parameter FWHM of silver is less than gold based sensor [46], [47], [48]. This result shows superior accuracy than gold. Compared to a gold-coated SPR sensor, a silver-coated SPR sensor has a better sensitivity. However, when in contact with the sensing medium, Ag's poor chemical stability causes oxidation and corrosion issues. There are numerous ways to increase the adsorption in order to get over these issues, including the use of nanoparticles and nanoholes, metallic nano slits, and biomolecular recognition elements (BRE) [46]. Ag layer with $d_{Ag} = 45$ nm thickness is constructed above the ZnO layer and used as the plasmonic layer due to its sharpest SPR peak, better sensitivity, and smaller FWHM.

The silicon is further deposited as the next layer over the Ag. A very thin Si layer thickness of $d_{Si} = 2$ nm is deposited by using the CVD method [50]. The Si layer enhances the mobility of the electrons and increase the ability to absorb maximum the light at resonance angle to produce a sharp resonance dip [51].

On the following layer, a monolayer Graphene nanosheet with a thickness of $d_G = 0.34$ nm is fabricated using the thermal chemical vapor deposition (CVD) method above the Si layer [50]. Graphene's unique structural, optical, and biocompatible property has attracted researchers in the field of biosensing [42]. Graphene is essentially a thin sheet of carbon atoms organized in a 2D honeycomb lattice [52]. Since graphene absorbs biomolecules more strongly due to the π-staking interaction in the hexagonal cells of grapheme and the carbon-based ring structure in biomolecules, the total sensitivity of the sensor is increased [53]. Graphene has been used in certain SPR experiments, and this data demonstrates that its high surface-to-volume ratio makes it an ideal platform for studying biomolecular interactions. As a result of its vast detection area and the ease with which a wide range of aromatic biomolecules may be uniformly functionalized via π-π contact (Van der Waals force), it is improving overall performance [49], [54]. Specifically, among extant nanomaterials, graphene has a surface area of 2,630 m^2/g and a rich π-conjugation structure, making it suitable for direct interaction with biomolecules [42], [55]. Moreover, graphene's large real component of dielectric constant allows it to effectively absorb the energy of incoming light. Up to 2.3% of incoming light is absorbed by monolayer graphene, and this percentage rises with the number of graphene layers. In the L layer of graphene, it can be as high as L×2.3% [56], [57]. Increased sensitivity in SPR-based sensors has been suggested as a potential use for graphene [58], [59]. Due to the fact that oxygen atoms cannot flow through 2D nanomaterials like graphene, which act like a shield the metallic layer from oxidation (environmental corrosion) [60], [61].

The last layer is a sensing medium. A cuvette is connected on top of the graphene layer. It provides a passage to the water sample to detect the salinity concentration. The variation of the refractive index of the sensing medium indicates the salinity concentration present in the water sample.

The performances of the proposed sensor are directly related to the possibility of the practical implementation and fabrication feasibility of the structure. The complexity of the design procedure and the manufacturing challenges are increasing the cost of the production. Due to recent developments of different nano scale fabrication techniques, the complex fabrication challenges are easily overcome and cost are minimized to acceptable range. In this work, a CaF_2 prism is used as a substrate. A ZnO layer can be uniformly deposit as a thin adhesion layer on the prism surface by using sol-gel spin coating method or ion plating sputtering technique [62], [63], [64]. The Ag layer is deposit as next layer about the ZnO layer, by using one of the different popular methods like - vacuum thermal coating procedure, activated reactive type physical vapor deposition (ARE-PVD) or vacuum evaporation-deposition [65], [66], [67]. A very thin Si layer is deposited above the Ag layer. A uniform Si nanolayer coating with high efficiency and little surface roughness can be achieved by using thermal chemical vapor deposition (CVD) method [68], [69]. A monolayer Graphene nanosheet with a thickness of $d_G = 0.34$ nm can be deposited using the thermal chemical vapor deposition (CVD) method above the Si layer [69], [70], [71]. All of those standard fabrication techniques are commercially available and mass amount of device production may be minimizing the design and fabrication cost.

The operational performance of a SPR sensor is highly depend on the thickness of the sensor. When an incident input light is applied to the surface of the prism coated with a thin metal layer at a resonance angle, a plasma is created due to oscillation of mobile electrons at the surface of the metal layer. Then the wave vector of the incident light matches the wavelength of the surface plasmons, the electrons resonate and an evanescent wave penetrates through the metal film. The amplitude of this evanescent field wave decreases exponentially with distance from the interface. The wavelength of the evanescent field wave is the same as that of the source incident light wavelength. The evanescent field decays over a distance of about one light

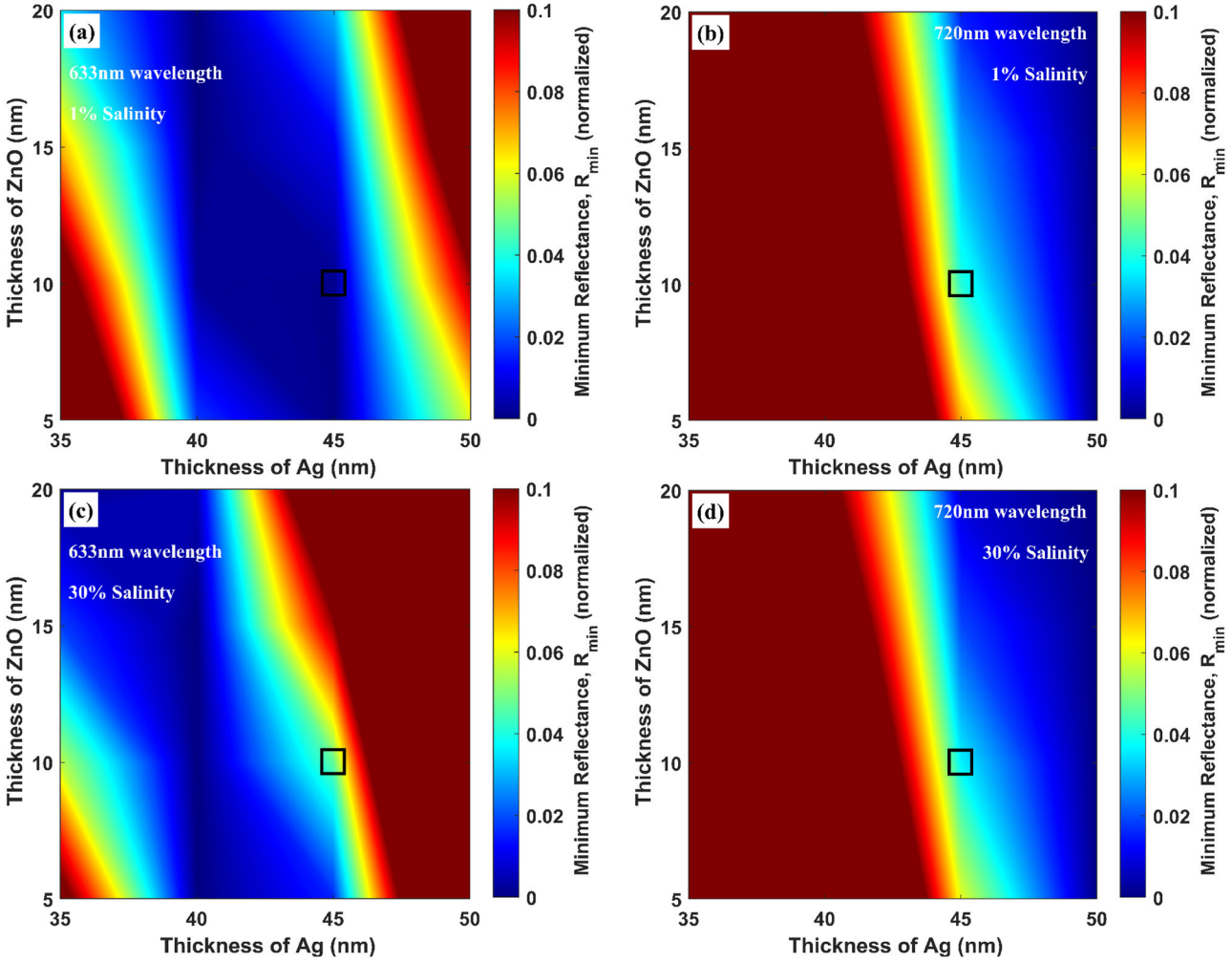

FIGURE 3. Thickness of ZnO and Ag layer variation based on minimum reflectance (R_{min}) considering Si (2nm), Graphene (0.34nm) layers are kept fixed (a) 633 nm wavelength source and 1% salinity, (b) 720 nm wavelength source and 1% salinity, (c) 633 nm wavelength source and 30% salinity, (d) 720 nm wavelength source and 30% salinity.

wavelength from the surface. Theoretically, an evanescent electrical field associated with the plasma wave travels for a short distance (∼300 nm) [72], [73]. Therefore, the proposed structure thickness of around 57.34nm with 633nm to 720nm wavelength light sources, the proposed sensor works perfectly without blocking any input laser light.

In addition, some of the research articles present a comparison of theoretical and experimental works. Those articles proposed a sensor with 40∼80nm Ag layer thickness and fabricated experimentally [65], [74], [75]. Another research article proposed a sensor with multilayer periodic structure of 230 nm thickness, which is analysis both theoretical and experimentally [76]. All of those research articles represent both theoretical and experimental results that are nearly identical [65], [74], [75], [76].

B. SPR SENSOR PARAMETERS

The proposed salinity concentration sensor consists of five different layers and measure the water sample salinity for five different incident light source wavelengths. All the performance parameters are measured and compared for five different light sources which increase the detection accuracy, reliability and overall performance of the biosensor. According to Cauchy equation - The refractive index of any material is related to its incident light wavelength (λ). The variation of the incident light wavelength (λ) can change the refractive index of any material [77]. The RI of CaF_2 prism is calculated by using following Equation (1), as shown at the bottom of the next page, which is related with wavelengths (λ) [61].

The refractive index of each layer such as ZnO, Ag, Si and Graphene thin layers are calculated and selected from verified experimental works to justify the feasibility of the sensor construction [78], [79], [80], [81], [82]. The refractive index of sensing mediums is varying from 1.33 to 1.33699 for water salinity concentration variation of 0% to 30% present in Table 1 [12]. In this work, the refractive index of the CaF_2 prism is 1.4329, 1.4327, 1.4321, 1.4318, and 1.4315 for 633nm, 643.8nm, 690nm, 700nm, and 720nm input light wavelength [61]. For the ZnO layer, the refractive index of the

ZnO layer is 1.9888, 1.9861, 1.9775, 1.9736, and 1.9701 for 633nm, 643.8nm, 690nm, 700nm, and 720nm input light wavelength [78].

According to the experimental works, the refractive indices of each other layers of the proposed structure are also varied with the input light wavelengths [77], [78], [79], [80], [81], [82]. This variation of the sensing medium RIs is measured for all five wavelengths (λ) of 633nm, 643.8nm, 690nm, 700nm, and 720nm of the incident light source. Fig. 2 represents the reflectivity (normalized) variation with incidence angle (deg.) curve for all five incident light wavelengths with 0% to 30% water salinity concentration variation. All those response curves obtain very low minimum reflectance below the normalized value of 0.05. The response curve of the proposed structure shows, the resonance angle for each incident light source moves to a higher value with increasing the salinity concentration. In addition, the resonance angle for each salinity concentration level move to a lower value with increasing the incident light source wavelengths (λ). For the 633 nm wavelength, the obtained resonance angle is 82.48° and 85.26°, which is a 2.78° variation for 0% to 30% water concentration variation. For 720 nm wavelength, the obtained resonance angle is 77.04° and 78.5°, which is a 1.46° variation for 0% to 30% water concentration variation. The sensitivity is defined as the ratio of the resonance angle shift with their corresponding refractive index variation. Therefore, the sensitivity of the proposed sensor is also varied with variations of the incident light source wavelengths (λ).

C. SPR SENSOR METHODOLOGY

Fig. 1 depicts the proposed structure for measuring the water salinity concentration with five monochromatic light sources of different wavelengths (λ) of 633nm, 643.8nm, 690nm, 700nm, and 720nm. To measure the water salinity, it is essential to detect and measure the absorption at resonance angle accurately. Therefore, the absorption is detected and analyzed using Fresnel multilayer reflection theory and the transfer matrix method (TMM). A CaF_2 based prism is proposed, and its reflection spectrum is analyzed numerically as the incoming photons travel through the structure. This establishes the concept of plasmon resonance at the surface of a prism metal (P-M) with evanescent wave (EW) accrete.

When an evanescent wave (EW) travelling in the x direction passes between ZnO and Ag layers, its incident wave vector (k_x) has a propagation constant (PC) in the x-direction. The resonant condition is sensitive to the incoming light angle θ. Equation (2) and Equation (3) describe the resonance condition, where the wave vector of SPs (k_{spwv}) coincides with the PC of the lowest reflection (k_x).

$$k_x = k_{spwv} \tag{2}$$

$$\frac{2\pi}{\lambda_{incident\ light}}\left(n_p sin\theta_{SPR}\right) = \frac{2\pi}{\lambda_{incident\ light}}\sqrt{\frac{n_{Ag}^2 n_s^2}{n_{Ag}^2 + n_s^2}} \tag{3}$$

The mathematical representation of SPR resonance angle (θ_{SPR}) expressed in Equation (4).

$$\theta_{SPR} = \left[sin\left(\sqrt{\frac{n_{Ag}^2 n_S^2}{n_{CaF_2}^2(n_{Ag}^2 + n_S^2)}}\right)\right]^{-1} \tag{4}$$

where n_{CaF2}, n_{Ag}, and n_S are the RI of CaF_2 prism, Ag layer and sensing medium, respectively. The angular modulation method is used to analyses the proposed structure. In addition, the reflectivity of P-polarized incident light wave was analyzed using the Fresnel multilayer reflection theory and the transfer matrix method. The surface plasmon resonance curve is a plot showing the relationship between the incidence angle (θ) and the sum of the reflected intensities (R_P) [80], [81]. Equation (5) and Equation (6) give the mathematical equation of total reflected intensity (R_P), and the reflection coefficient (q_P):

$$R_p = q_p q_p^* = \left|q_p\right|^2 \tag{5}$$

$$q_p = \frac{(M_{11} + M_{12}n_N) - (M_{21} + M_{22}n_N)}{(M_{11} + M_{12}n_N) + (M_{21} + M_{22}n_N)} \tag{6}$$

where M is the SPR sensor's characteristics matrix [83], [84]. Equation (7) and Equation (8) provide a description of the transverse RI and characteristics matrix, respectively.

$$n_k = \sqrt{\left(\begin{bmatrix}\mu_k\\ \varepsilon_k\end{bmatrix}\right)} \quad \cos\theta_k = \sqrt{\frac{\varepsilon_k - \left(n_p sin\theta\right)^2}{\varepsilon_k^2}} \tag{7}$$

$$M_{if} = \left[\prod_{k=2}^{N-1}\begin{pmatrix} cos\beta_k & -i\,sin\beta_k \\ -in_k sin\beta_k & \cos\beta_k\end{pmatrix}\right]_{if} = \begin{bmatrix} M_{11} & M_{12} \\ M_{21} & M_{22}\end{bmatrix} \tag{8}$$

In addition, the kth layer's arbitrary stage constant (β_k) and wave impedance (z_k) can be calculated using Equation (9) and Equation (10), respectively [85].

$$\beta_k = \frac{2\pi}{\lambda} n_k \cos\theta_k\,(z_k - z_{k-1}) = \frac{2\pi}{\lambda} d_k \sqrt{\varepsilon_k - \left(n_p sin\theta\right)^2} \tag{9}$$

$$z_k = \frac{k_x n_k cos\theta_k}{\left(2\pi c/\lambda_{incidentlight}\right)\varepsilon_k^2} \tag{10}$$

$$n_{CaF_2} = \left(\frac{0.567588\lambda^2}{\lambda^2 - 0.050263^2} + \frac{0.4710914\lambda^2}{\lambda^2 - 0.10039^2} + \frac{3.8484723\lambda^2}{\lambda^2 - 34.64904^2} + 1\right)^{\frac{1}{2}} \tag{1}$$

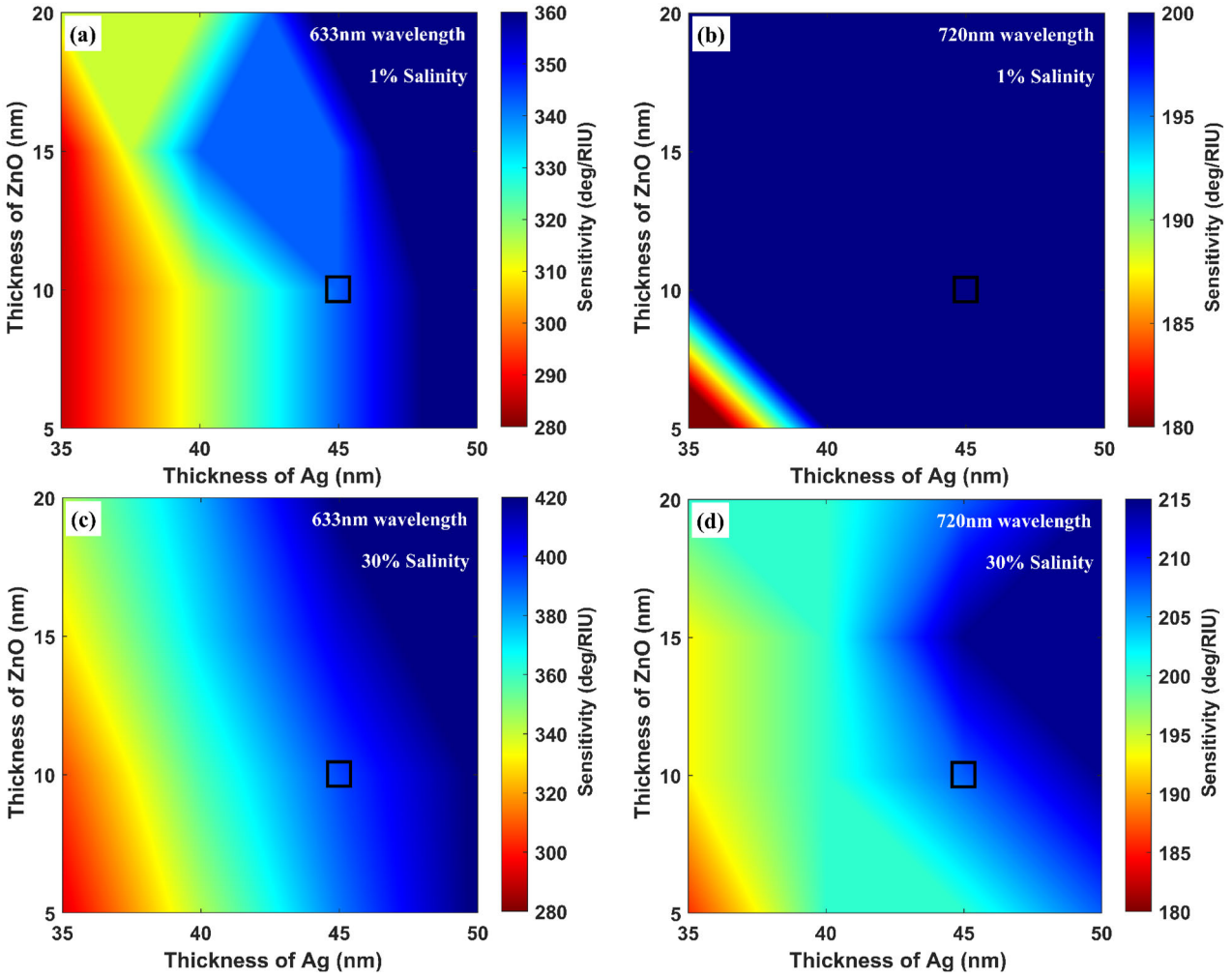

FIGURE 4. Thickness of ZnO and Ag layer variation based on sensitivity (S) considering Si (2nm), Graphene (0.34nm) layers are kept fixed (a) 633 nm wavelength source and 1% salinity, (b) 720 nm wavelength source and 1% salinity, (c) 633 nm wavelength source and 30% salinity, (d) 720 nm wavelength source and 30% salinity.

where ε_k and d_k stand for the kth layer's permittivity and thickness, respectively. Finally, we can calculate the kth layer's input angle θ_k as:

$$\theta_k = \frac{1}{\cos\left(\sqrt{1 - \left({}^{n_{k-1}}/_{n_k}\right)(sin\theta)^2}\right)} \tag{11}$$

D. SPR PERFORMANCE PARAMETER

Sensitivity (S) is one of the most essential performance evaluation parameters for SPR biosensors. The ratio of the resonance angle ($\Delta\theta_{res}$) variation with rescpect to the change in the RI (Δn) is used to determine the sensitivity. Equation (12) defined sensitivity as.

$$S = \frac{\Delta\theta_{res}}{\Delta n} \tag{12}$$

To evaluate the overall efficacy of SPR sensors, a number of additional crucial factors must be considered. Full width at half maximum (FWHM), Quality Factor (QF), Figure of Merit (FOM), and Detection Accuracy (DA) are frequently used to evaluate the performance of SPR sensors [10], [11]. These parameters are described as follows -

$$FWHM = (\theta_{max} - \theta_{min}) \tag{13}$$

$$QF = \frac{S}{FWHM} \tag{14}$$

$$FOM = S \times \frac{1 - R_{min}}{FWHM} \tag{15}$$

$$DA = \frac{1}{FWHM} \tag{16}$$

E. SENSOR CALIBRATION, MAINTENANCE AND OPERATIONAL RANGE

The specific target of this work is to design a highly accurate and sensitive SPR sensor for water salinity detection. For this reason, the proposed sensor is designed by analysis and calibrated with a known data set for accurate detection, and precision measurement, and obtained very high overall

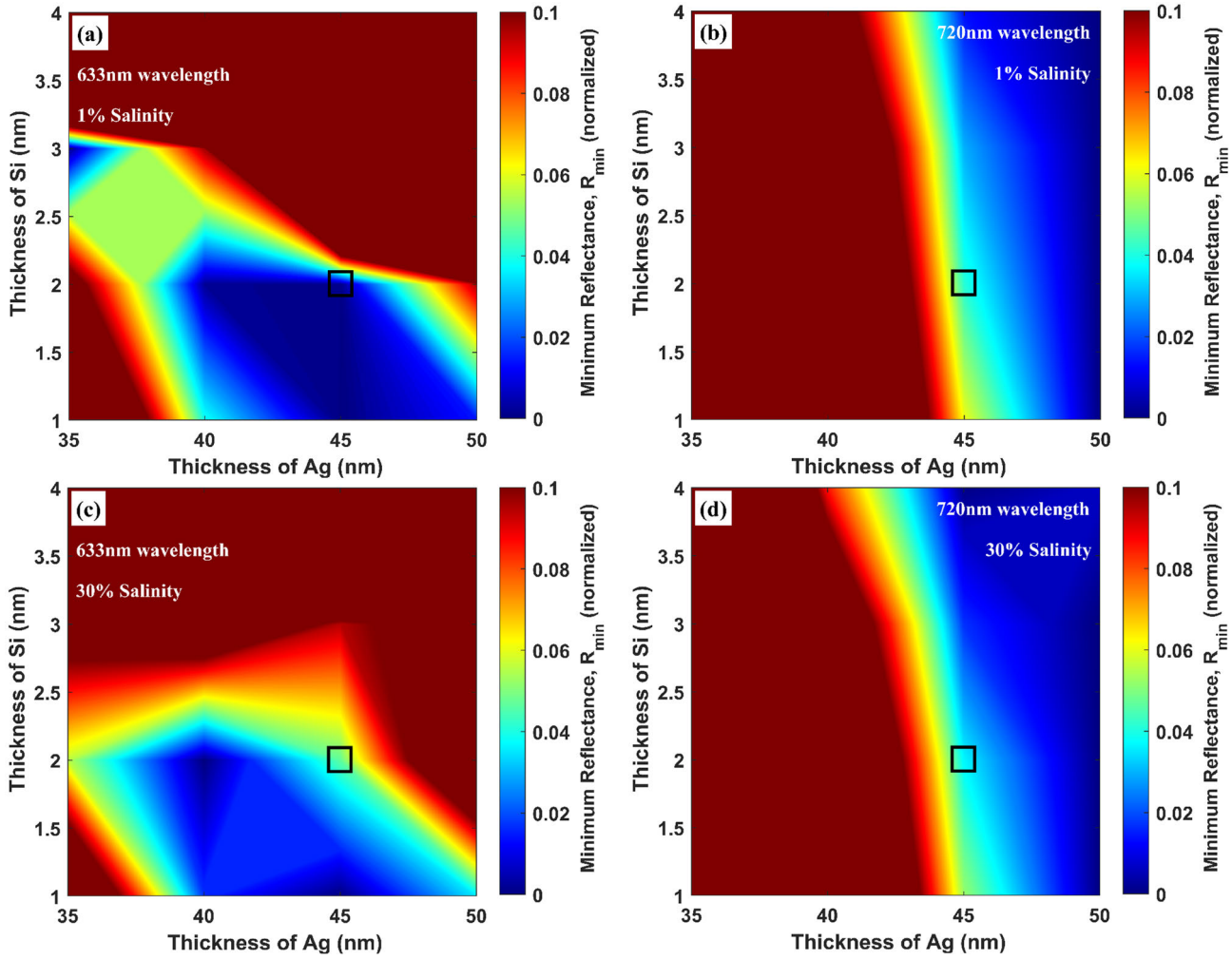

FIGURE 5. Thickness of Ag and Si layer variation based on minimum reflectance considering ZnO (10nm), Graphene (0.34nm) layers are kept fixed (a) 633 nm wavelength source and 1% salinity, (b) 720 nm wavelength source and 1% salinity, (c) 633 nm wavelength source and 30% salinity, (d) 720 nm wavelength source and 30% salinity.

performance parameters for the applied water sample. The maximum accurate detection range of this sensor is 0% to 30% water salinity concentration, which is related 1.33 to 1.33699 refractive index variation of the applied water sample. The proposed sensor can be used to detect and measure any other object within the range of the refractive index of the sample between 1.33 to 1.33699. Due to the optimization of the sensor for only water salinity detection, these refractive index ranges limit the detection range and accuracy of the proposed sensor for other object detection rather than water salinity.

Furthermore, if considering the water sample containing other elements, or interfering with unwanted elements such as chemical or biological agents, due to this condition the sensor-obtained results may be varied differently for different wavelengths of the input light sources. Because of the presence of unknown or unwanted elements in the sample water, the refractive index of the applied sample varied by different random values for all five input wavelengths. The measured data is now compared with the premeasured calibrated data and the calculated percentage of salinity concentration with a finite accuracy range. Therefore, in this condition, the measuring accuracy may be decreased but the probable value of the concentration level can be measured.

The durability of any device is a very important factor for long-term use. Regular maintenance increases the performance and longevity of the device. The proposed sensor device can be used multiple times with high durability. No further calibration and maintenance are needed for multiple or long-term uses. Before using the sensor, the sensing layer only needs to be cleaned by using acetone or purified water as regular maintenance. Which indicates very low operational costs and very high usability in any environment.

The power consumption of the sensor related to the laser sources, reflected light detector and the processing unit. Due to advance of modern electronics, all of these components are operating around 6 to 12 volts DC supply with very

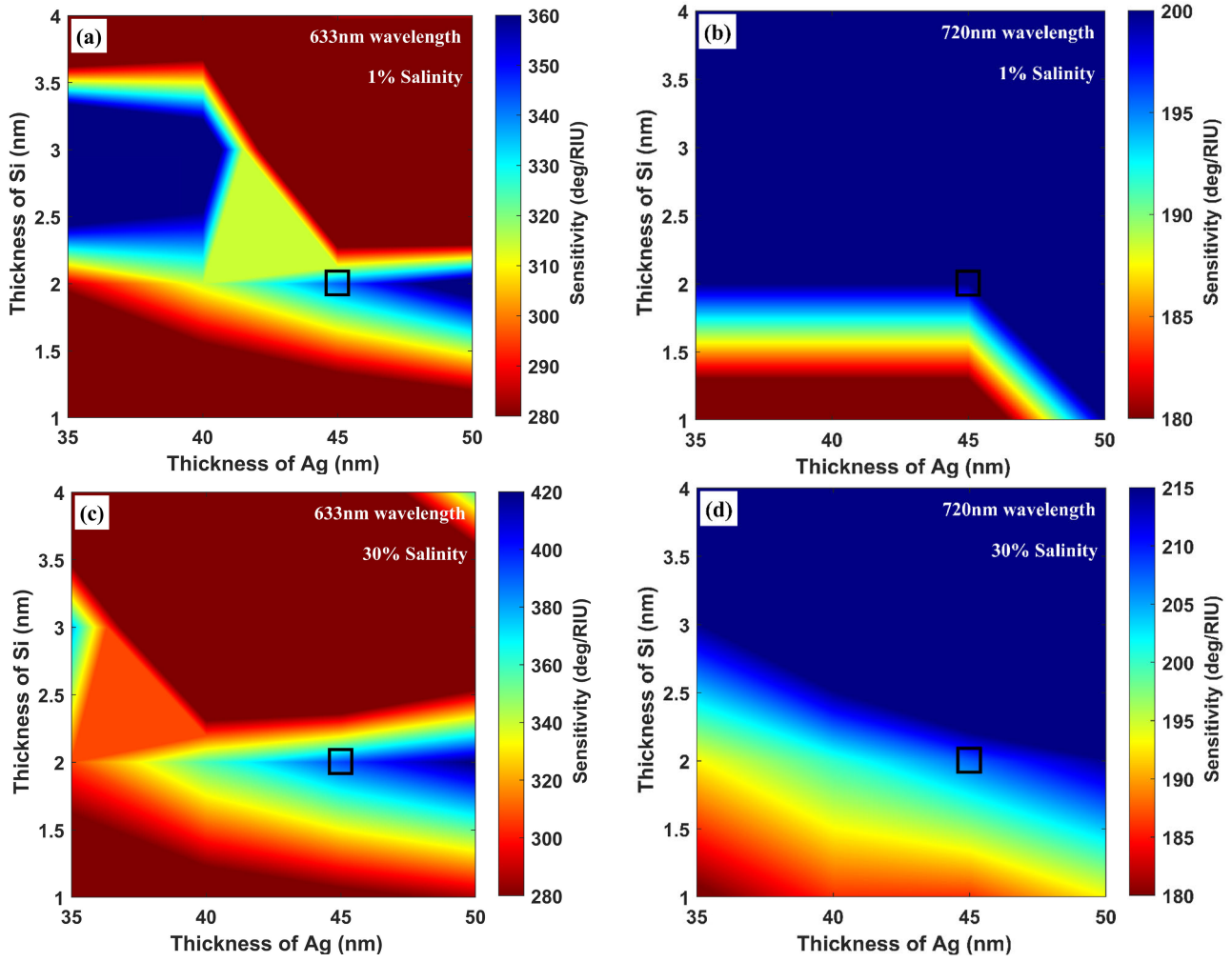

FIGURE 6. Thickness of Ag and Si layer variation based on sensitivity considering ZnO (10nm), Graphene (0.34nm) layers are kept fixed (a) 633 nm wavelength source and 1% salinity, (b) 720 nm wavelength source and 1% salinity, (c) 633 nm wavelength source and 30% salinity, (d) 720 nm wavelength source and 30% salinity.

low amount of power consumption. Therefore, the proposed sensor can be used as a portable device to measure the water salinity concentration level.

III. OPTIMIZATION AND ANALYSIS OF DIFFERENT PERFORMANCE PARAMETERS

In this section, the optimal thickness of each layer is determined by observing the effect on the performance parameters of the proposed device. The different performance parameters such as Minimum Reflectance (R_{min}), Sensitivity (S), Quality factor (QF), etc. are considered to identify the optimum thickness of each layer. Using angular interrogation method and MATLAB iterative simulation, the optimum thickness is determined by measuring the minimum reflectance (R_{min}). Here, the proposed structure is design considering the value of R_{min} less than 0.05 (normalized) with achieving highest possible all others performance parameters. The ANSYS Lumerical simulator was used to conduct A Finite-Difference Time-Domain (FDTD) analysis, which confirmed the accuracy of the analytical solution obtained by means of the Transfer Matrix Method (TMM). The outcomes from the two approaches were virtually identical.

A. THICKNESS OPTIMIZATION OF DIFFERENT LAYER

The performances of any sensor are depending on various performance parameters such as Sensitivity, Minimum Reflectance, Full width at half maximum, Quality factor, Figure of Merit, Detection Accuracy, etc. In addition to enhanced the overall performance with maintaining the range of the parameters, the structure needs to be optimized by considering all performance parameters. The proposed structure is based on five different layers including the prism. Therefore, author optimized the proposed structure thickness by considering all performance parameters using iterative optimization method. Here, presented variation of R_{min} and S for minimum and maximum salinity concentration level which is 0% and 30% with lower (633nm) to higher (720nm)

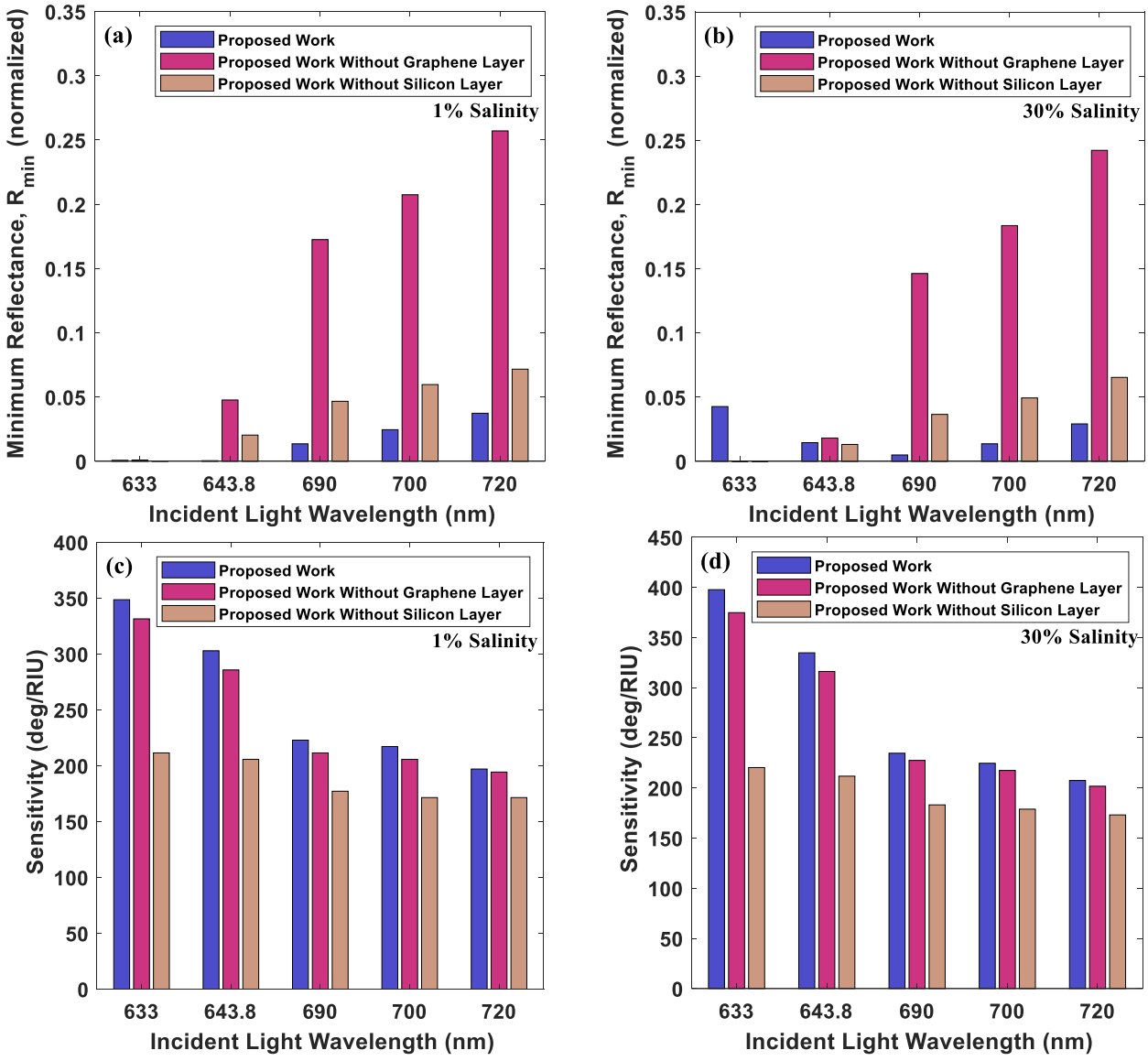

FIGURE 7. The impact of graphene and silicon layers on the proposed sensor (a) minimum reflectance versus incident light wavelength for 1% water salinity concentration, (b) minimum reflectance versus incident light wavelength for 30% water salinity concentration, (c) sensitivity versus incident light wavelength for 1% water salinity concentration, (d) sensitivity versus incident light wavelength for 30% water salinity concentration.

incident light source wavelengths (λ). Here, the proposed structure is design considering the value of R_{min} less than 0.05 (normalized value) or 5% with achieving higher all others performance parameters.

Fig. 3 and Fig. 4 shows the optimization of ZnO and Ag layers based on the R_{min} and S. Both figures show, the minimum reflectance with optimum sensitivity achieved for ZnO layer at thickness of $d_{ZnO} = 10$ nm and Ag layer at thickness of $d_{Ag} = 45$ nm, considering Si ($d_{Si} = 2$ nm) and Graphene ($d_G = 0.34$ nm) layers are kept fixed. Fig. 3 shows, the R_{min} is much more sensitive with Ag layer thickness compare to ZnO layer thickness. Fig. 4 shows, the S is increasing with increasing both Ag and ZnO layer thickness.

Fig. 5 and Fig. 6 shows the optimization of Ag and Si layers based on the minimum reflectance and sensitivity, considering Ag ($d_{Ag} = 45\,nm$) and Graphene ($d_G = 0.34\,nm$) layers are kept fixed. Fig. 5(a) and Fig. 5(c) shows, the R_{min} is much more sensitive with Si layer thickness compare to Ag layer thickness, when the incident light source wavelength is 633nm. Fig. 5(b) and Fig. 5(d) shows, when the incident light source wavelength is 720 nm the R_{min} is more sensitive with Ag layer thickness compare to Si layer thickness. Fig. 6 shows, the S is increasing with increasing both Ag and ZnO layer thickness. Despite the fact that, the S is decreasing with changing the thickness of Ag layer at thickness of $d_{Ag} = 45$ nm and Si layer at thickness of $d_{Si} = 2$ nm shown in Fig. 6(a) and Fig. 6(c). Therefore, the minimum reflectance

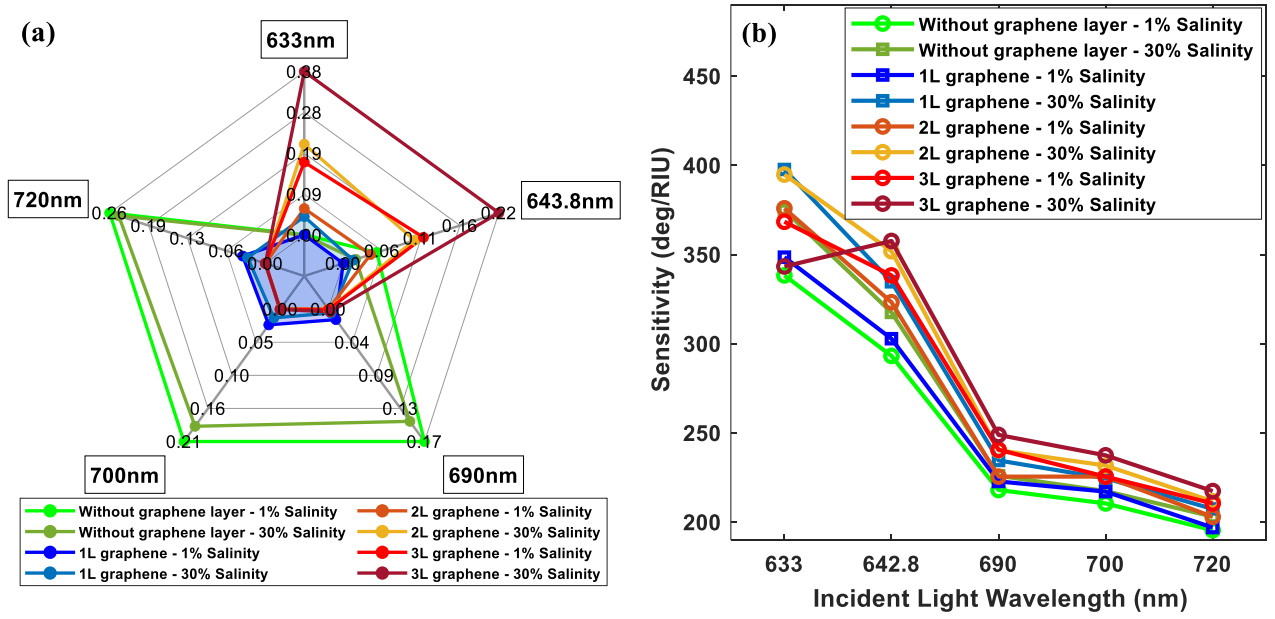

FIGURE 8. Variation of graphene layers with incident light wavelengths, (a) minimum reflectance, and (b) sensitivity.

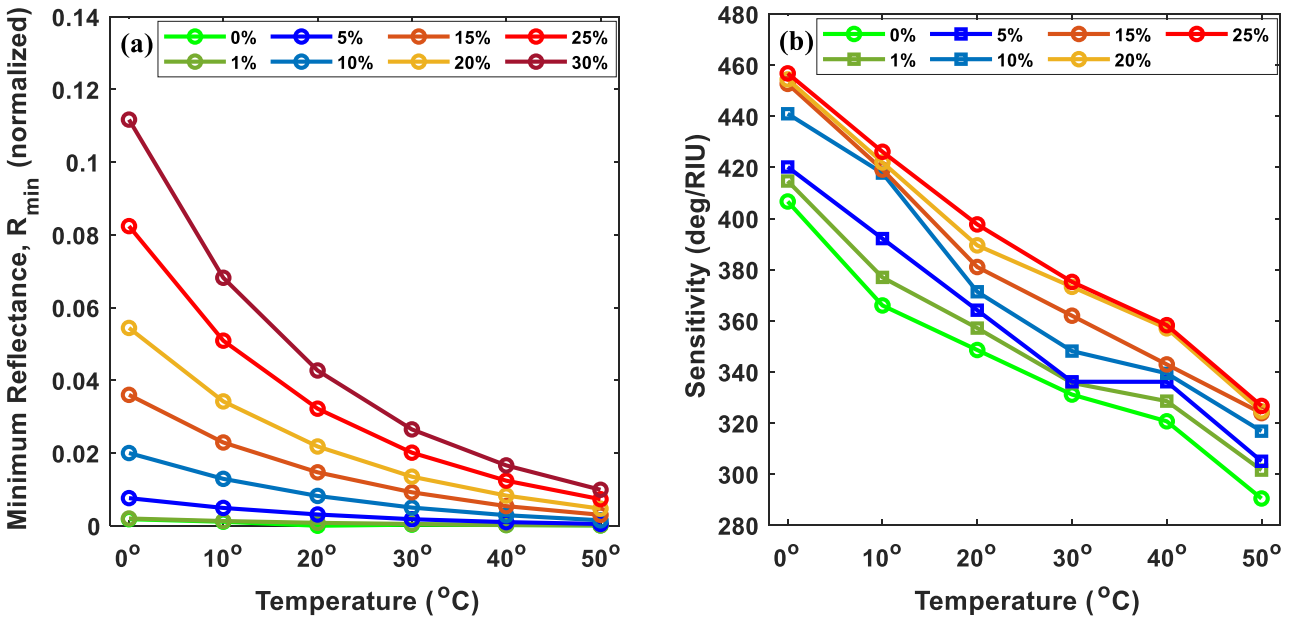

FIGURE 9. Temperature variation of proposed sensor, (a) minimum reflectance, and (b) sensitivity.

with optimum sensitivity achieved for Ag layer at thickness of $d_{Ag} = 45\ nm$ and Si layer at thickness of $d_{Si} = 2$ nm.

B. IMPACT OF GRAPHENE AND SILICON LAYER

The graphene creates a significant impact on sensitivity as well as on minimum reflectance. Graphene layers or silicon layers can be used to increase the sensitivity of a sensor, which has been already mentioned and analysed by many research articles [53], [86]. The impact of graphene and silicon layers on the proposed sensor is presented graphically in Fig. 7. The minimum reflectance and sensitivity of the proposed structure are compared with the 'proposed structure without graphene layer' and 'proposed structure without silicon layer' to investigate the impact of graphene and silicon layer. Fig. 7(a) and Fig. 7(b) presents the minimum reflectance versus incident light wavelength for 1% and 30% water salinity concentration. The figure shows very low minimum reflectance when both silicon and graphene are considered as a part of the proposed structure. Without a graphene layer, the value of minimum reflectance is very

TABLE 2. Minimum Reflectance and Full Width at Half Maximum of the proposed sensor at different wavelengths and water salinity concentration.

Salinity	Minimum Reflectance (normalized)					Full Width at Half Maximum (deg)				
(%)	633 nm	643.8 nm	690 nm	700 nm	720 nm	633 nm	643.8 nm	690 nm	700 nm	720 nm
0%	0.0000	0.0000	0.0142	0.0249	0.0398	4.33	3.64	2.54	2.27	1.95
1%	0.0008	0.0005	0.0136	0.0246	0.0374	4.41	3.70	2.49	2.30	1.98
5%	0.0031	0.0013	0.0141	0.0256	0.0361	4.48	3.77	2.54	2.32	2.04
10%	0.0082	0.0026	0.0147	0.0266	0.0348	4.56	3.84	2.54	2.34	2.05
15%	0.0147	0.0045	0.0131	0.0249	0.0334	4.66	3.93	2.57	2.37	2.07
20%	0.0218	0.0071	0.0098	0.0207	0.0319	4.79	4.02	2.61	2.40	2.10
25%	0.0322	0.0108	0.0070	0.0168	0.0304	4.93	4.11	2.65	2.44	2.13
30%	0.0427	0.0146	0.0050	0.0137	0.0292	5.03	4.19	2.69	2.47	2.15

TABLE 3. Sensitivity and Detection Accuracy of the proposed sensor at different wavelengths and water salinity concentration.

Salinity	Sensitivity (deg./RIU)					Detection Accuracy (1/deg.)				
(%)	633 nm	643.8 nm	690 nm	700 nm	720 nm	633 nm	643.8 nm	690 nm	700 nm	720 nm
1%	348.57	302.86	222.86	217.14	197.00	0.2260	0.2702	0.4016	0.4347	0.4975
5%	357.14	308.27	223.80	218.05	199.25	0.2232	0.2652	0.3968	0.4310	0.4901
10%	364.15	310.92	226.89	218.49	201.68	0.2192	0.2604	0.3937	0.4273	0.4878
15%	371.36	317.67	228.19	219.24	203.58	0.2145	0.2544	0.3891	0.4219	0.4830
20%	381.04	323.42	230.48	221.19	204.46	0.2087	0.2487	0.3831	0.4166	0.4761
25%	389.51	329.09	232.11	222.58	206.68	0.2028	0.2433	0.3773	0.4098	0.4694
30%	397.71	334.76	234.62	224.61	207.44	0.1988	0.2386	0.3717	0.4048	0.4651

TABLE 4. Quality factor and Figure of Merit of the proposed sensor at different wavelengths and water salinity concentration.

Salinity	Quality factor (1/RIU)					Figure of Merit				
(%)	633 nm	643.8 nm	690 nm	700 nm	720 nm	633 nm	643.8 nm	690 nm	700 nm	720 nm
1%	79.04	81.85	89.50	94.41	99.50	78.97	81.82	87.86	91.46	94.82
5%	79.72	81.77	88.02	93.98	97.67	79.42	81.68	86.37	90.97	93.23
10%	79.86	80.97	89.33	93.37	98.38	79.09	80.78	87.61	90.29	94.07
15%	79.69	80.83	88.79	92.51	98.35	78.33	80.48	87.25	89.65	94.22
20%	79.55	80.45	88.31	92.16	97.36	77.51	79.87	87.13	89.76	93.45
25%	79.01	80.07	87.59	91.22	97.03	76.00	79.17	86.72	89.25	93.32
30%	79.07	79.90	87.22	90.93	96.48	75.04	78.67	86.58	89.30	92.93

high and increases rapidly with the increase of incident light wavelength. This is not acceptable for any sensor design. Without a silicon layer, the minimum reflectance is a slightly higher value compared with the proposed structure. This indicates that using a silicon layer also reduces the value of minimum reflectance and improves the sensor performance. Fig. 7(c) and Fig. 7(d) represent the sensitivity versus incident light wavelength for 1% and 30% water salinity concentration. Both figures show the proposed structure obtained the highest value for all salinity concentrations including for all five incident light wavelengths. The structure without a graphene layer shows lower values of sensitivity for all cases compared to the proposed structure. Therefore, using a graphene layer increased the sensitivity of the proposed structure.

C. PERFORMANCE ANALYSIS OF MULTIPLE GRAPHENE LAYERS

Many researchers already focus on Graphene-based structures for sensors due to many promising advantages. Graphene layers are used to increase the sensitivity of the sensors. Fig. 8(a) shows the minimum reflectance variation with incident light wavelength for different numbers of graphene layers. The sensor without a graphene layer obtains larger R_{min} for higher incident light wavelengths, which is a 0.17 to 0.29 normalized value. On the other side, the proposed sensor with two and three graphene layers shows much higher R_{min} for lower incident light wavelengths. This R_{min} is decreasing with the increase of the incident light wavelengths. Here, only single graphene layer-based structure shows an overall low R_{min} for any incident light wavelengths with maintaining a higher sensitivity. Fig. 8(b) represents the sensitivity of the sensor for graphene layer variation. The S is moving to a higher value with an increment of the graphene layer. In the meantime, the S is starting to decrease with increasing the incident light wavelengths. Therefore, a single graphene layer is selected for the sensor to obtain a balanced low R_{min} with maintaining a higher S.

D. EFFECT OF TEMPERATURE VARIATION

Temperature is an essential factor in any device performance. In this work, a 20°C fixed temperature is considered for all salinity concentration levels and five different wavelengths of incident light sources. The literature review, for 633nm wavelength the refractive index of water varies from 1.333 to 1.3174 for 0°C to 100°C temperature variation [87]. Here,

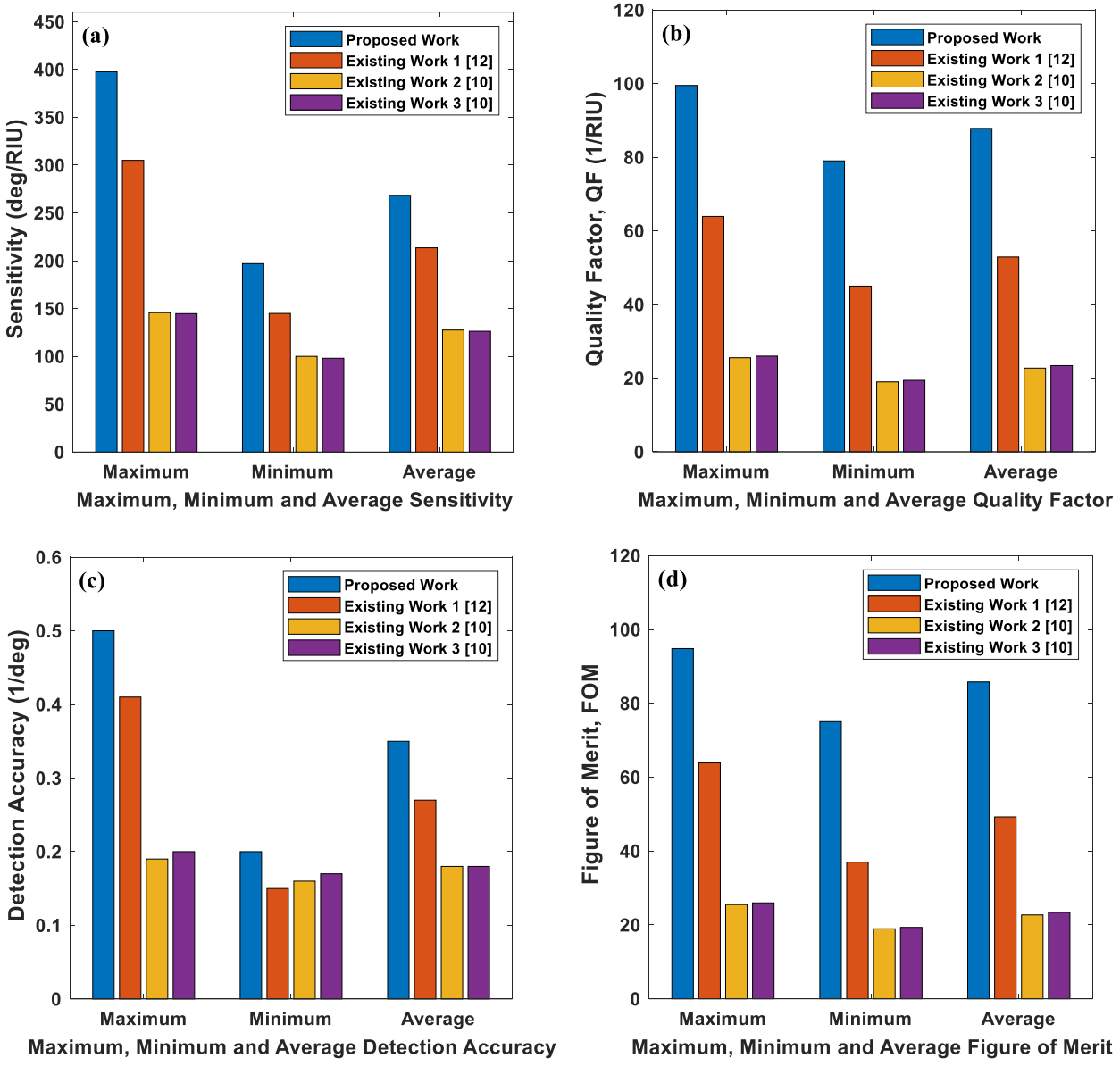

FIGURE 10. Comparison between proposed sensor performance with recent existing (a) sensitivity, (b) quality factor, (c) detection accuracy and, (d) figure of merit.

for 1°C temperature variation, the refractive index varies 0.000156 or 0.0156% only. The refractive index of each layer also varies with temperature variation [71], [88], [89], [90], [91], [92], [93], [94]. The variation of sensor performance with temperature variation is presented in Fig. 9 (a) and Fig. 9(b).

Fig. 9(a) shows, that the minimum reflectance of the sensor is sensitive to temperature variation for all salinity concentration levels. The value of minimum reflectance of the proposed sensor is slightly higher when the sensor operates near 0°C temperature. The value of minimum reflectance decreases exponentially with increasing the sensor operating temperature. Fig. 9(b) shows the sensitivity of the sensor decreases with increasing the sensor operating temperature for all salinity concentration levels. Considering both response curves, the proposed sensor obtained the best measuring performance when the device operates between 15°C to 40°C temperature.

IV. RESULTS ANALYSIS AND PERFORMANCE COMPARISON

The different performance parameters such as R_{min}, $FWHM$, S, DA, QF and FOM of proposed SPR-based water salinity concentration sensor are presented in Table 2-4. All those performance parameters are measured for salinity concentration variation of 0% to 30% including the incident light source wavelength variation of 633nm to 720nm. For 633 nm wavelength, the obtained resonance angle is 82.48°

and 85.26°, which is 2.78° variation for 0% to 30% water concentration variation. Here the resonance angle varies by 0.092° for per percentile concentration variation. For 720 nm wavelength, the obtained resonance angle is 77.04° and 78.5°, which is a 1.46° variation for 0% to 30% water concentration variation. Therefore, the resonance angle varies by 0.048° for per percentile concentration variation. For both lower and higher input wavelengths, those values are significantly higher compared with relevant reference works [10], [12]. In addition, those values also showed higher values as compared to other recent SPR sensor devices [14], [27], [48], [51].

From Table 2, the result shows that, the R_{min} for all measured condition is lower than 0.05 (normalized) value, which is one of the required conditions for accurate detection. Table 3 represent that, the S of the proposed sensor is increase with salinity concentration increases and decrease with incident light source wavelength increases. Furthermore, the DA the proposed sensor is decrease with salinity concentration increases and increase with incident light source wavelength increase. The observation of other performance parameters such as QF and FOM are represent in Table 4. The results show, QF and FOM are almost same value due to very low value R_{min}. Both QF and FOM are nearly same value with salinity concentration variation, and increase with incident light source wavelength increases.

The comparison of performance parameters of proposed water salinity concentration sensor with recent related works are presented in Fig. 10(a) to Fig. 10(d). All those performance parameters are compared for maximum to minimum range including the average values of all measured condition. Fig. 10(a) shows that, the proposed sensor achieved 30.4% to 35.96%, 97% to 172.91% and 100.94% to 174.5% increased S compared to existing work 1, existing work 2 and existing work 3. Fig. 10(b) present that, the proposed SPR sensor is more selective and accurate for detection due to 55.67% to 75.57%, 289.75% to 316.49% and 283.14% to 307.47% higher QF compared to existing work 1, 2 and 3, respectively.

The proposed structure obtained 0.199 to 0.498 (deg^{-1}) DA which is 21.34% to 32.53%, 23.48% to 159.11% and 19.04% to 153.83% enhanced range compared to existing work 1, 2 and 3, respectively. The detection accuracy is directly related to the angle difference of a particular reflectivity curve when a sample is applied to the sensor for measurement with a single input source. For any sensor, a high value of detection accuracy means sharper the SPR spectral curve which indicates more reliability and accuracy of the device for measurement or detection. In addition, the detection accuracy is not only measuring or detecting parameters used for measurement and detection. For accurate detection with precision measurement, all other parameters such as Sensitivity, Minimum reflectance, Quality Factor, and Figure of Merit are also simultaneously measured. All measured parameters are compared with pre-measured data for final output.

The FOM factor is depending on both Minimum Reflectance and Quality factor. Table 2-4 shows, the structure obtained very low R_{min} which is below 5% for all measuring condition. As a result, the sensor achieved higher value of FOM which is 48.48% to 102.82%, 271.68% to 296.01% and 265.1% to 288.22% enhanced compared to existing work 1, 2 and 3, respectively. Therefore, the proposed SPR salinity concentration sensor is shows very high overall performance with working five different input source wavelengths which make the sensor much more accurate, efficient, reliable to detect water salinity concentration.

V. CONCLUSION

In this work, a new Graphene-based surface plasmon resonance sensor is presented for rapid water salinity concentration detection. The proposed sensor is optimised to operate for five different wavelength of input light sources. This new multiple source technique significantly increases the detection precision of the sensor, and meantime improve the overall performance of the sensor to detect the water salinity concentration. The sensor can detect water salinity concentration of any water sample by measuring different performance parameters and compare with previously measured data to identify the salinity level with high accuracy. The proposed SPR sensor achieved very high Sensitivity of a range of 197 to 397.71 (deg./RIU) with maintaining very low minimum reflectance, which is 0.05 (normalized) for whole salinity detection range. The sensor attains higher range of Quality Factor as 79.01 to 99.50 (1/RIU) and Figure of Merit of 75.04 to 94.82, due to very low value of minimum reflectance. The sensor also covers a wide range of detection accuracy of 0.199 to 0.498 (1/deg.), which is significantly higher value compare to the relevant recent works. Additionally, the proposed sensor demonstrated remarkably improved overall performances with five times increased detection precision compared to recent sensors. Therefore, this proposed SPR-based sensor for measuring the salinity level of water exhibited highest sensitivity, quality factor, figure of merit and detection accuracy.

ACKNOWLEDGMENT

The authors would like to thank the support and facilities provided by BUET.

REFERENCES

[1] C. J. Lote, *Principles of Renal Physiology*. New York, NY, USA: Springer, 2013, pp. 1–204, doi: 10.1007/978-1-4614-3785-7.

[2] M. Elimelech, "The global challenge for adequate and safe water," *J. Water Supply, Res. Technol. Aqua*, vol. 55, no. 1, pp. 3–10, Feb. 2006, doi: 10.2166/aqua.2005.064.

[3] X. Xu, A. E. Allah, C. Wang, H. Tan, A. A. Farghali, M. H. Khedr, V. Malgras, T. Yang, and Y. Yamauchi, "Capacitive deionization using nitrogen-doped mesostructured carbons for highly efficient brackish water desalination," *Chem. Eng. J.*, vol. 362, pp. 887–896, Apr. 2019, doi: 10.1016/j.cej.2019.01.098.

[4] M. Mengel, A. Levermann, K. Frieler, A. Robinson, B. Marzeion, and R. Winkelmann, "Future sea level rise constrained by observations and long-term commitment," *Proc. Nat. Acad. Sci. USA*, vol. 113, no. 10, pp. 2597–2602, Mar. 2016, doi: 10.1073/pnas.1500515113.

[5] H. Etesami and F. Noori, *Saline Soil-Based Agriculture by Halotolerant Microorganisms*. Singapore: Springer, 2019, pp. 1–22, doi: 10.1007/978-981-13-8335-9.

[6] F. Adamo, F. Attivissimo, C. G. C. Carducci, and A. M. L. Lanzolla, "A smart sensor network for sea water quality monitoring," *IEEE Sensors J.*, vol. 15, no. 5, pp. 2514–2522, May 2015, doi: 10.1109/JSEN.2014.2360816.

[7] Y. Qian, Y. Zhao, Q.-L. Wu, and Y. Yang, "Review of salinity measurement technology based on optical fiber sensor," *Sens. Actuators B, Chem.*, vol. 260, pp. 86–105, May 2018, doi: 10.1016/j.snb.2017.12.077.

[8] L. Xia, S. Yin, H. Gao, Q. Deng, and C. Du, "Sensitivity enhancement for surface plasmon resonance imaging biosensor by utilizing gold-silver bimetallic film configuration," *Plasmonics*, vol. 6, no. 2, pp. 245–250, Jun. 2011, doi: 10.1007/s11468-010-9195-y.

[9] Q. Wu, L. Wang, H. Zhang, J. Deng, Y. Zhao, J. Liu, J. Xiang, and S. Wu, "Strong coupling of excitons in monolayer WS_2 with guided-mode resonance," *Results Phys.*, vol. 44, Jan. 2023, Art. no. 106191, doi: 10.1016/j.rinp.2022.106191.

[10] S. Raikwar, Y. K. Prajapati, D. K. Srivastava, and J. P. Saini, "Graphene oxide based SPR sensor for sensing of sea water concentration," *Results Opt.*, vol. 1, Nov. 2020, Art. no. 100011, doi: 10.1016/j.rio.2020.100011.

[11] K. M. Ishtiak, S.-A. Imam, and Q. D. M. Khosru, "$BaTiO_3$—Blue Phosphorus/WS_2 hybrid structure-based surface plasmon resonance biosensor with enhanced sensor performance for rapid bacterial detection," *Results Eng.*, vol. 16, Dec. 2022, Art. no. 100698, doi: 10.1016/j.rineng.2022.100698.

[12] B. Hossain, A. K. Paul, M. A. Islam, M. F. Hossain, and M. M. Rahman, "Design and analysis of highly sensitive prism based surface plasmon resonance optical salinity sensor," *Results Opt.*, vol. 7, May 2022, Art. no. 100217, doi: 10.1016/j.rio.2022.100217.

[13] C. Gao and Y. Zhang, "Seawater refractive index sensor based on a cascaded double grating structure," *Opt. Mater.*, vol. 142, Aug. 2023, Art. no. 114011, doi: 10.1016/j.optmat.2023.114011.

[14] Md. A. Islam, A. K. Paul, B. Hossain, A. K. Sarkar, M. M. Rahman, A. S. M. Sayem, R. B. V. B. Simorangkir, M. A. Shobug, J. L. Buckley, K. Chakrabarti, and A. Lalbakhsh, "Design and analysis of GO coated high sensitive tunable SPR sensor for OATR spectroscopic biosensing applications," *IEEE Access*, vol. 10, pp. 103496–103508, 2022, doi: 10.1109/ACCESS.2022.3211099.

[15] Md. S. Islam, C. M. B. Cordeiro, J. Sultana, R. A. Aoni, S. Feng, R. Ahmed, M. Dorraki, A. Dinovitser, B. W. Ng, and D. Abbott, "A hi-bi ultra-sensitive surface plasmon resonance fiber sensor," *IEEE Access*, vol. 7, pp. 79085–79094, 2019, doi: 10.1109/ACCESS.2019.2922663.

[16] H. Sayed and A. H. Aly, "Salinity optical sensor by using two-dimensional photonic crystals: Computational study," *Mater. Sci. Eng., B*, vol. 269, Jul. 2021, Art. no. 115169, doi: 10.1016/j.mseb.2021.115169.

[17] A. K. Sharma and A. K. Pandey, "Blue Phosphorene/MoS_2 heterostructure based SPR sensor with enhanced sensitivity," *IEEE Photon. Technol. Lett.*, vol. 30, no. 7, pp. 595–598, Apr. 1, 2018, doi: 10.1109/LPT.2018.2803747.

[18] S.-A. Imam, K. M. Ishtiak, and Q. D. M. Khosru, "Modelling a near perfect temperature tunable multiband VO_2 based photonic-plasmonic absorber within visible and near infrared spectra," *Results Eng.*, vol. 18, Jun. 2023, Art. no. 101084, doi: 10.1016/j.rineng.2023.101084.

[19] K. Liu, J. Zhang, J. Jiang, T. Xu, S. Wang, P. Chang, Z. Zhang, J. Ma, and T. Liu, "$MoSe_2$-Au based sensitivity enhanced optical fiber surface plasmon resonance biosensor for detection of Goat-anti-Rabbit IgG," *IEEE Access*, vol. 8, pp. 660–668, 2020, doi: 10.1109/ACCESS.2019.2961751.

[20] Md. A. Mollah, H. Sarker, M. Ahsan, M. T. Elahi, M. A. Based, J. Haider, and S. Palani, "Designing highly sensitive surface plasmon resonance sensor with dual analyte channels," *IEEE Access*, vol. 9, pp. 139293–139302, 2021, doi: 10.1109/ACCESS.2021.3118927.

[21] S.-A. Imam, K. M. Ishtiak, and Q. D. M. Khosru, "Graphene-VO_2-based-defect-induced tunable multiple narrowband unidirectional photonic terahertz absorber," *Opt. Mater. Exp.*, vol. 12, no. 7, p. 2653, 2022, doi: 10.1364/ome.462860.

[22] H. Fu, S. Zhang, H. Chen, and J. Weng, "Graphene enhances the sensitivity of fiber-optic surface plasmon resonance biosensor," *IEEE Sensors J.*, vol. 15, no. 10, pp. 5478–5482, Oct. 2015, doi: 10.1109/JSEN.2015.2442276.

[23] S. Pal, A. Verma, Y. K. Prajapati, and J. P. Saini, "Influence of black phosphorous on performance of surface plasmon resonance biosensor," *Opt. Quantum Electron.*, vol. 49, no. 12, p. 403, Dec. 2017, doi: 10.1007/s11082-017-1237-7.

[24] F. A. Said, P. S. Menon, T. Kalaivani, M. A. Mohamed, A. Abedini, S. Shaari, B. Y. Majlis, and V. Retnasamy, "FDTD analysis of structured metallic nanohole films for LSPR-based biosensor," in *Proc. IEEE Regional Symp. Micro Nanoelectronics (RSM)*, Aug. 2015, pp. 1–4, doi: 10.1109/RSM.2015.7355024.

[25] M. Biednov, T. Lebyedyeva, and P. Shpylovyy, "Gold and aluminum based surface plasmon resonance biosensors: Sensitivity enhancement," *Proc. SPIE*, vol. 9506, May 2015, Art. no. 95061P, doi: 10.1117/12.2177992.

[26] A. K. Mishra, S. K. Mishra, and R. K. Verma, "Graphene and beyond graphene MoS_2: A new window in surface-plasmon-resonance-based fiber optic sensing," *J. Phys. Chem. C*, vol. 120, no. 5, pp. 2893–2900, Feb. 2016, doi: 10.1021/acs.jpcc.5b08955.

[27] M. M. Rahman, L. F. Abdulrazak, M. Ahsan, M. A. Based, M. M. Rana, M. S. Anower, K. A. Rikta, J. Haider, and S. Gurusamy, "2D nanomaterial-based hybrid structured (Au-WSe_2-$PtSe_2$-BP) surface plasmon resonance (SPR) sensor with improved performance," *IEEE Access*, vol. 10, pp. 689–698, 2022, doi: 10.1109/ACCESS.2021.3137420.

[28] T. B. A. Akib, S. Mostufa, M. M. Rana, M. B. Hossain, and M. R. Islam, "A performance comparison of heterostructure surface plasmon resonance biosensor for the diagnosis of novel coronavirus SARS-CoV-2," *Opt. Quantum Electron.*, vol. 55, no. 5, p. 448, May 2023, doi: 10.1007/s11082-023-04700-4.

[29] S. Pal, Y. K. Prajapati, and J. P. Saini, "Influence of graphene's chemical potential on SPR biosensor using ZnO for DNA hybridization," *Opt. Rev.*, vol. 27, no. 1, pp. 57–64, Feb. 2020, doi: 10.1007/s10043-019-00564-w.

[30] A. Panda and P. D. Pukhrambam, "Modeling of high-performance SPR refractive index sensor employing novel 2D materials for detection of malaria pathogens," *IEEE Trans. Nanobiosci.*, vol. 21, no. 2, pp. 312–319, Apr. 2022, doi: 10.1109/TNB.2021.3115906.

[31] R. Nuryadi and R. D. Mayasari, "ZnO/Au-based surface plasmon resonance for CO_2 gas sensing application," *Appl. Phys. A, Solids Surf.*, vol. 122, no. 1, p. 33, Jan. 2016, doi: 10.1007/s00339-015-9536-y.

[32] A. Uniyal, B. Chauhan, A. Pal, and Y. Singh, "Surface plasmon biosensor based on Bi_2Te_3 antimonene heterostructure for the detection of cancer cells," *Appl. Opt.*, vol. 61, no. 13, pp. 3711–3719, 2022, doi: 10.1364/ao.454789.

[33] S. Singh, A. K. Sharma, P. Lohia, D. K. Dwivedi, V. Kumar, and P. K. Singh, "Simulation study of reconfigurable surface plasmon resonance refractive index sensor employing bismuth telluride and MXene nanomaterial for cancer cell detection," *Phys. Scripta*, vol. 98, no. 2, Feb. 2023, Art. no. 025813, doi: 10.1088/1402-4896/acb023.

[34] S. Mostufa, A. K. Paul, and K. Chakrabarti, "Detection of hemoglobin in blood and urine glucose level samples using a graphene-coated SPR based biosensor," *OSA Continuum*, vol. 4, no. 8, p. 2164, 2021, doi: 10.1364/osac.433633.

[35] A. Yadav, A. Kumar, P. Sharan, K. Manchikalapati, and S. Talabattula, "2-D transition metal dichalcogenides assisted SPR biosensor for rapid detection of urine glucose," *Proc. SPIE*, vol. 12159, Jan. 2022, Art. no. 1215903, doi: 10.1117/12.2624207.

[36] M. M. Hossain and M. A. Talukder, "Gate-controlled graphene surface plasmon resonance glucose sensor," *Opt. Commun.*, vol. 493, Aug. 2021, Art. no. 126994, doi: 10.1016/j.optcom.2021.126994.

[37] Y. Zhao, Z.-Q. Deng, and Q. Wang, "Fiber optic SPR sensor for liquid concentration measurement," *Sens. Actuators B, Chem.*, vol. 192, pp. 229–233, Mar. 2014, doi: 10.1016/j.snb.2013.10.108.

[38] A. Yadav, A. Kumar, and P. Sharan, "Sensitivity enhancement of a plasmonic biosensor for urine glucose detection by employing black phosphorous," *J. Opt. Soc. Amer. B, Opt. Phys.*, vol. 39, no. 1, pp. 200–206, 2022, doi: 10.1364/josab.444838.

[39] S. Cho, Y. Lee, H. Koh, H. Jung, J. Kim, H. Yoo, J. Kim, and H. Jung, "Superior chemical sensing performance of black phosphorus: Comparison with MoS_2 and graphene," *Adv. Mater.*, vol. 28, no. 32, pp. 7020–7028, Aug. 2016, doi: 10.1002/adma.201601167.

[40] A. K. Sharma and A. Dominic, "Influence of chemical potential on graphene-based SPR sensor's performance," *IEEE Photon. Technol. Lett.*, vol. 30, no. 1, pp. 95–98, Jan. 1, 2018, doi: 10.1109/LPT.2017.2776945.

[41] R. Kumar, A. S. Kushwaha, M. Srivastava, H. Mishra, and S. K. Srivastava, "Enhancement in sensitivity of graphene-based zinc oxide assisted bimetallic surface plasmon resonance (SPR) biosensor," *Appl. Phys. A, Solids Surf.*, vol. 124, no. 3, p. 235, Mar. 2018, doi: 10.1007/s00339-018-1606-5.

[42] A. Kumar, A. K. Yadav, A. S. Kushwaha, and S. K. Srivastava, "A comparative study among WS_2, MoS_2 and graphene based surface plasmon resonance (SPR) sensor," *Sensors Actuators Rep.*, vol. 2, no. 1, Nov. 2020, Art. no. 100015, doi: 10.1016/j.snr.2020.100015.

[43] L. A. Walsh, R. Addou, R. M. Wallace, and C. L. Hinkle, "Molecular beam epitaxy of transition metal dichalcogenides," in *Molecular Beam Epitaxy*. Amsterdam, The Netherlands: Elsevier, 2018, doi: 10.1016/b978-0-12-812136-8.00024-4.

[44] R. Arat, G. Jia, J. Dellith, A. Dellith, and J. Plentz, "Solution processed transparent conductive hybrid thin films based on silver nanowires, zinc oxide and graphene," *Mater. Today Commun.*, vol. 26, Mar. 2021, Art. no. 102162, doi: 10.1016/j.mtcomm.2021.102162.

[45] K. Khurana and N. Jaggi, "Localized surface plasmonic properties of Au and Ag nanoparticles for sensors: A review," *Plasmonics*, vol. 16, no. 4, pp. 981–999, Aug. 2021, doi: 10.1007/s11468-021-01381-1.

[46] A. Verma, A. Prakash, and R. Tripathi, "Sensitivity enhancement of surface plasmon resonance biosensor using graphene and air gap," *Opt. Commun.*, vol. 357, pp. 106–112, Dec. 2015, doi: 10.1016/j.optcom.2015.08.076.

[47] A. K. Sharma, R. Jha, and B. D. Gupta, "Fiber-optic sensors based on surface plasmon resonance: A comprehensive review," *IEEE Sensors J.*, vol. 7, no. 8, pp. 1118–1129, Aug. 2007, doi: 10.1109/jsen.2007.897946.

[48] M. M. Rahman, M. M. Rana, M. S. Rahman, M. S. Anower, M. A. Mollah, and A. K. Paul, "Sensitivity enhancement of SPR biosensors employing heterostructure of $PtSe_2$ and 2D materials," *Opt. Mater.*, vol. 107, Sep. 2020, Art. no. 110123, doi: 10.1016/j.optmat.2020.110123.

[49] L. Wu, H. S. Chu, W. S. Koh, and E. P. Li, "Highly sensitive graphene biosensors based on surface plasmon resonance," *Opt. Exp.*, vol. 18, no. 14, p. 14395, 2010, doi: 10.1364/oe.18.014395.

[50] H. Matsumura, "Catalytic chemical vapor deposition (CTC-CVD) method producing high quality hydrogenated amorphous silicon," *Jpn. J. Appl. Phys.*, vol. 25, no. 12, pp. 949–951, Dec. 1986, doi: 10.1143/jjap.25.l949.

[51] Y. Vasimalla, H. S. Pradhan, and R. J. Pandya, "Sensitivity enhancement of the SPR biosensor for pseudomonas bacterial detection employing a silicon-barium titanate structure," *Appl. Opt.*, vol. 60, no. 19, p. 5588, 2021, doi: 10.1364/ao.427499.

[52] M. Biabanifard, A. Arsanjani, M. S. Abrishamian, and D. Abbott, "Tunable terahertz graphene-based absorber design method based on a circuit model approach," *IEEE Access*, vol. 8, pp. 70343–70354, 2020, doi: 10.1109/ACCESS.2020.2986682.

[53] M. S. Islam, J. Sultana, M. Biabanifard, Z. Vafapour, M. J. Nine, A. Dinovitser, C. M. B. Cordeiro, B. W.-H. Ng, and D. Abbott, "Tunable localized surface plasmon graphene metasurface for multiband superabsorption and terahertz sensing," *Carbon*, vol. 158, pp. 559–567, Mar. 2020, doi: 10.1016/j.carbon.2019.11.026.

[54] B. Song, D. Li, W. Qi, M. Elstner, C. Fan, and H. Fang, "Graphene on Au(111): A highly conductive material with excellent adsorption properties for high-resolution bio/nanodetection and identification," *ChemPhysChem*, vol. 11, no. 3, pp. 585–589, Feb. 2010, doi: 10.1002/cphc.200900743.

[55] G. B. McGaughey, M. Gagné, and A. K. Rappé, "π-stacking interactions," *J. Biol. Chem.*, vol. 273, no. 25, pp. 15458–15463, Jun. 1998, doi: 10.1074/jbc.273.25.15458.

[56] R. Verma, B. D. Gupta, and R. Jha, "Sensitivity enhancement of a surface plasmon resonance based biomolecules sensor using graphene and silicon layers," *Sens. Actuators B, Chem.*, vol. 160, no. 1, pp. 623–631, Dec. 2011, doi: 10.1016/j.snb.2011.08.039.

[57] A. B. Kuzmenko, E. van Heumen, F. Carbone, and D. van der Marel, "Universal optical conductance of graphite," *Phys. Rev. Lett.*, vol. 100, no. 11, Mar. 2008, Art. no. 117401, doi: 10.1103/physrevlett.100.117401.

[58] M. B. Hossain and M. M. Rana, "Graphene coated high sensitive surface plasmon resonance biosensor for sensing DNA hybridization," *Sensor Lett.*, vol. 14, no. 2, pp. 145–152, Feb. 2016, doi: 10.1166/sl.2016.3596.

[59] S. H. Choi, Y. L. Kim, and K. M. Byun, "Graphene-on-silver substrates for sensitive surface plasmon resonance imaging biosensors," *Opt. Exp.*, vol. 19, no. 2, p. 458, 2011, doi: 10.1364/oe.19.000458.

[60] P. K. Maharana, R. Jha, and S. Palei, "Sensitivity enhancement by air mediated graphene multilayer based surface plasmon resonance biosensor for near infrared," *Sens. Actuators B, Chem.*, vol. 190, pp. 494–501, Jan. 2014, doi: 10.1016/j.snb.2013.08.089.

[61] I. H. Malitson, "A redetermination of some optical properties of calcium fluoride," *Appl. Opt.*, vol. 2, no. 11, p. 1103, 1963, doi: 10.1364/ao.2.001103.

[62] M. A. Chougule, S. Sen, and V. B. Patil, "Fabrication of nanostructured ZnO thin film sensor for NO_2 monitoring," *Ceram. Int.*, vol. 38, no. 4, pp. 2685–2692, May 2012, doi: 10.1016/j.ceramint.2011.11.036.

[63] S. L. Patil, M. A. Chougule, S. G. Pawar, B. T. Raut, S. Sen, and V. B. Patil, "New process for synthesis of ZnO thin films: Microstructural, optical and electrical characterization," *J. Alloys Compounds*, vol. 509, no. 41, pp. 10055–10061, Oct. 2011, doi: 10.1016/j.jallcom.2011.08.030.

[64] T. Terasako, Y. Ochi, M. Yagi, J. Nomoto, and T. Yamamoto, "Structural and optical properties of ZnO films grown on ion-plated Ga doped ZnO buffer layers by atmospheric-pressure chemical vapor deposition using Zn and H_2O as source materials," *Thin Solid Films*, vol. 663, pp. 79–84, Oct. 2018, doi: 10.1016/j.tsf.2018.07.050.

[65] S. Agarwal, P. Giri, Y. K. Prajapati, and P. Chakrabarti, "Effect of surface roughness on the performance of optical SPR sensor for sucrose detection: Fabrication, characterization, and simulation study," *IEEE Sensors J.*, vol. 16, no. 24, pp. 8865–8873, Dec. 2016, doi: 10.1109/JSEN.2016.2615110.

[66] E. Thouti, N. Chander, V. Dutta, and V. K. Komarala, "Optical properties of Ag nanoparticle layers deposited on silicon substrates," *J. Opt.*, vol. 15, no. 3, Mar. 2013, Art. no. 035005, doi: 10.1088/2040-8978/15/3/035005.

[67] D. J. J. Hu and H. P. Ho, "Recent advances in plasmonic photonic crystal fibers: Design, fabrication and applications," *Adv. Opt. Photon.*, vol. 9, no. 2, p. 257, 2017, doi: 10.1364/aop.9.000257.

[68] T. S. Drake, C. N. Chléirigh, M. L. Lee, A. J. Pitera, E. A. Fitzgerald, D. A. Antoniadis, D. H. Anjum, J. Li, R. Hull, N. Klymko, and J. L. Hoyt, "Fabrication of ultra-thin strained silicon on insulator," *J. Electron. Mater.*, vol. 32, no. 9, pp. 972–975, Sep. 2003, doi: 10.1007/s11664-003-0232-x.

[69] A. T. Smith, A. M. LaChance, S. Zeng, B. Liu, and L. Sun, "Synthesis, properties, and applications of graphene oxide/reduced graphene oxide and their nanocomposites," *Nano Mater. Sci.*, vol. 1, no. 1, pp. 31–47, Mar. 2019, doi: 10.1016/j.nanoms.2019.02.004.

[70] L. G. De Arco, Y. Zhang, A. Kumar, and C. Zhou, "Synthesis, transfer, and devices of single- and few-layer graphene by chemical vapor deposition," *IEEE Trans. Nanotechnol.*, vol. 8, no. 2, pp. 135–138, Mar. 2009, doi: 10.1109/tnano.2009.2013620.

[71] S. Wu, L. Wan, L. Wei, D. N. Talwar, K. He, and Z. Feng, "Temperature-dependent optical properties of graphene on Si and SiO_2/Si substrates," *Crystals*, vol. 11, no. 4, p. 358, Mar. 2021, doi: 10.3390/cryst11040358.

[72] A. H. P. Ho, D. Kim, and M. G. Somekh, *Handbook of Photonics for Biomedical Engineering*. Dordrecht, The Netherlands: Springer, 2017, doi: 10.1007/978-94-007-5052-4.

[73] P. A. V. Der Merwe, "Surface plasmon resonance," in *Protein-Ligand Interactions: Hydrodynamics and Calorimetry*. New York, NY, USA: Oxford Univ. Press, 2001, pp. 137–170. [Online]. Available: http://agure.bilkent.edu.tr/13SurfacePlasmonResonance-generalinfo.pdf

[74] Y. Dai, H. Xu, H. Wang, Y. Lu, and P. Wang, "Experimental demonstration of high sensitivity for silver rectangular grating-coupled surface plasmon resonance (SPR) sensing," *Opt. Commun.*, vol. 416, pp. 66–70, Jun. 2018, doi: 10.1016/j.optcom.2018.02.010.

[75] V. Kapoor, N. K. Sharma, and V. Sajal, "Indium tin oxide and silver based fiber optic SPR sensor: An experimental study," *Opt. Quantum Electron.*, vol. 51, no. 4, p. 125, Apr. 2019, doi: 10.1007/s11082-019-1837-5.

[76] C.-W. Lin, K.-P. Chen, C.-N. Hsiao, S. Lin, and C.-K. Lee, "Design and fabrication of an alternating dielectric multi-layer device for surface plasmon resonance sensor," *Sens. Actuators B, Chem.*, vol. 113, no. 1, pp. 169–176, Jan. 2006, doi: 10.1016/j.snb.2005.02.044.

[77] F. Jenkins and H. E. White, *Fundamentals of Optics*, 4th ed. New York, NY, USA: McGraw-Hill, 1981. [Online]. Available: https://handoutset.com/wp-content/uploads/2022/07/Fundamentals-of-optics-Francis-Jenkins-Harvey-White.pdf

[78] O. Aguilar, S. de Castro, M. P. F. Godoy, and M. R. S. Dias, "Opto-electronic characterization of $Zn_{1-x}Cd_xO$ thin films as an alternative to photonic crystals in organic solar cells," *Opt. Mater. Exp.*, vol. 9, no. 9, p. 3638, 2019, doi: 10.1364/ome.9.003638.

[79] P. B. Johnson and R. W. Christy, "Optical constants of the noble metals," *Phys. Rev. B, Condens. Matter*, vol. 6, no. 12, pp. 4370–4379, Dec. 1972.

[80] D. E. Aspnes and A. A. Studna, "Dielectric functions and optical parameters of Si, Ge, GaP, GaAs, GaSb, InP, InAs, and InSb from 1.5 to 6.0 eV," *Phys. Rev. B, Condens. Matter*, vol. 27, no. 2, pp. 985–1009, Jan. 1983, doi: 10.1103/physrevb.27.985.
[81] Y. Cao, E. Hu, J. Xing, L. Liu, T. Gu, J. Zheng, K. Yu, and W. Wei, "Optical constants of restored and etched reduced graphene oxide: A spectroscopic ellipsometry study," *Opt. Mater. Exp.*, vol. 9, no. 1, p. 234, 2019, doi: 10.1364/ome.9.000234.
[82] S. H. Wemple, M. Didomenico, and I. Camlibel, "Dielectric and optical properties of melt-grown $BaTiO_3$," *J. Phys. Chem. Solids*, vol. 29, no. 10, pp. 1797–1803, Oct. 1968, doi: 10.1016/0022-3697(68)90164-9.
[83] M. S. Rahman, M. S. Anower, L. F. Abdulrazak, and M. M. Rahman, "Modeling of a fiber-optic surface plasmon resonance biosensor employing phosphorene for sensing applications," *Opt. Eng.*, vol. 58, no. 3, p. 1, Mar. 2019, doi: 10.1117/1.oe.58.3.037103.
[84] M. B. Hossain, M. M. Islam, L. F. Abdulrazak, M. M. Rana, T. B. A. Akib, and M. Hassan, "Graphene-coated optical fiber SPR biosensor for BRCA1 and BRCA2 breast cancer biomarker detection: A numerical design-based analysis," *Photonic Sensors*, vol. 10, no. 1, pp. 67–79, Mar. 2020, doi: 10.1007/s13320-019-0556-7.
[85] M. S. Rahman, M. S. Anower, M. R. Hasan, M. B. Hossain, and M. I. Haque, "Design and numerical analysis of highly sensitive Au-MoS_2-graphene based hybrid surface plasmon resonance biosensor," *Opt. Commun.*, vol. 396, pp. 36–43, Aug. 2017, doi: 10.1016/j.optcom.2017.03.035.
[86] D. T. Nurrohman and N.-F. Chiu, "A review of graphene-based surface plasmon resonance and surface-enhanced Raman scattering biosensors: Current status and future prospects," *Nanomaterials*, vol. 11, no. 1, p. 216, Jan. 2021, doi: 10.3390/nano11010216.
[87] A. N. Bashkatov and E. A. Genina, "Water refractive index in dependence on temperature and wavelength: A simple approximation," *Proc. SPIE*, vol. 5068, pp. 393–395, Oct. 2003, doi: 10.1117/12.518857.
[88] I. Thormählen, J. Straub, and U. Grigull, "Refractive index of water and its dependence on wavelength, temperature, and density," *J. Phys. Chem. Reference Data*, vol. 14, no. 4, pp. 933–945, Oct. 1985, doi: 10.1063/1.555743.
[89] R. M. Waxler and G. W. Cleek, "The effect of temperature and pressure on the refractive index of some oxide glasses," *J. Res. Nat. Bur. Standards Sect. A, Phys. Chem.*, vol. 77, no. 6, p. 755, Nov. 1973, doi: 10.6028/jres.077a.046.
[90] H. H. Li, "Refractive index of alkaline earth halides and its wavelength and temperature derivatives," *J. Phys. Chem. Reference Data*, vol. 9, no. 1, pp. 161–290, Jan. 1980, doi: 10.1063/1.555616.
[91] D. B. Leviton, K. H. Miller, M. A. Quijada, and F. U. Grupp, "Temperature-dependent refractive index measurements of CaF_2, Suprasil 3001, and S-FTM16 for the Euclid near-infrared spectrometer and photometer," *Proc. SPIE*, vol. 9578, Sep. 2015, Art. no. 95780M, doi: 10.1117/12.2189024.
[92] M. Schmid, S. Zehnder, P. Schwaller, B. Neuenschwander, M. Held, U. Hunziker, and J. Zürcher, "Measuring optical properties on rough and liquid metal surfaces," *ALT Proc.*, vol. 1, pp. 277–278, Nov. 2012, doi: 10.12684/alt.1.78.
[93] O. Yavas, N. Do, A. C. Tam, P. T. Leung, W. P. Leung, H. K. Park, C. P. Grigoropoulos, J. Boneberg, and P. Leiderer, "Temperature dependence of optical properties for amorphous silicon at wavelengths of 6328 and 752 nm," *Opt. Lett.*, vol. 18, no. 7, p. 540, 1993, doi: 10.1364/ol.18.000540.
[94] Y. S. Park and J. R. Schneider, "Index of refraction of ZnO," *J. Appl. Phys.*, vol. 39, no. 7, pp. 3049–3052, Jun. 1968, doi: 10.1063/1.1656731.

KHANDAKAR MOHAMMAD ISHTIAK received the B.Sc. degree in electrical and electronic engineering (EEE) from the Ahsanullah University of Science and Technology (AUST), Dhaka, Bangladesh, in 2008, and the M.Sc. degree in EEE from the Islamic University of Technology (IUT), Gazipur, Bangladesh, in 2016. He is currently pursuing the Ph.D. degree with the Department of Electrical and Electronic Engineering, Bangladesh University of Engineering and Technology (BUET). He is also an Assistant Professor with the EEE Department, AUST. His research interests include photonics, 2D material-based optoelectronics, SPR-based biosensors, and nanodevices.

SAFAYAT-AL IMAM (Member, IEEE) received the B.Sc. degree in electrical and electronic engineering (EEE) from the Ahsanullah University of Science and Technology (AUST), Dhaka, Bangladesh, in 2008, and the M.A.Sc. degree in ECE from Concordia University, Canada, in 2013. He is currently pursuing the Ph.D. degree with the Department of Electrical and Electronic Engineering, Bangladesh University of Engineering and Technology. Since 2014, he has been an Assistant Professor with the EEE Department, AUST. He has published numerous articles in various national and international IEEE sponsored conferences. His research interests include photonics, 2D material-based optoelectronics, SPR-based biosensors, and phase change material (PCM)-based devices.

QUAZI D. M. KHOSRU received the B.Sc. degree in electrical and electronic engineering from Aligarh Muslim University, Aligarh, India, in 1986, the M.Sc. degree in electrical and electronic engineering from the Bangladesh University of Engineering and Technology (BUET), Dhaka, Bangladesh, in 1989, and the Ph.D. degree in electronic engineering from Osaka University, Osaka, Japan, in 1994. He was with NCR Corporation, Bangladesh, for a short period after graduation. He joined the Department of Electrical and Electronic Engineering, Bangladesh University of Engineering and Technology, as a Lecturer, in July 1987, and became a Professor, in May 2000. He was an Associate Professor with the Abdus Salam International Center for Theoretical Physics, Trieste, Italy, for a period of six years, from January 1996 to December 2001. He was a Visiting Research Scholar with Tohoku University, Sendai, Japan, from 1999 to 2000, and a Visiting Professor with the Research Center for Nanodevices and Systems, Hiroshima University, Hiroshima, Japan, from 2000 to 2002. He is also working in the area of nanophotonic materials and devices. He was the Chairman of the IEEE Electron Devices Society Bangladesh Chapter, in 2010, and several times in subsequent years. He was also the Chairman of the IEEE Bangladesh Section, in 2007 and 2017. He is the current Dean of the Faculty of Electrical and Electronic Engineering, BUET. He has published and presented over 200 technical papers in international journals and conferences. His research interests include nanodevice reliability, quantum mechanical modeling, reliability of high-κ dielectrics, physics, modeling and characterization of novel nanoscale MOS devices, junction-less transistor, and 2-D material devices.